

University of Mississippi

eGrove

Faculty and Student Publications

Engineering, School of

2-1-2020

Detrital zircon provenance and lithofacies associations of montmorillonitic sands in the maastrichtian ripley formation: Implications for mississippi embayment paleodrainage patterns and paleogeography

Jennifer N. Gifford

University of Mississippi

Elizabeth J. Vitale

University of Mississippi

Brian F. Platt

University of Mississippi

David H. Malone

Illinois State University

Inoka H. Widanagamage

University of Mississippi

Follow this and additional works at: https://egrove.olemiss.edu/engineering_facpubs



Recommended Citation

Gifford, J. N., Vitale, E. J., Platt, B. F., Malone, D. H., & Widanagamage, I. H. (2020). Detrital Zircon Provenance and Lithofacies Associations of Montmorillonitic Sands in the Maastrichtian Ripley Formation: Implications for Mississippi Embayment Paleodrainage Patterns and Paleogeography. *Geosciences*, 10(2), 80. <https://doi.org/10.3390/geosciences10020080>

This Article is brought to you for free and open access by the Engineering, School of at eGrove. It has been accepted for inclusion in Faculty and Student Publications by an authorized administrator of eGrove. For more information, please contact egrove@olemiss.edu.

Article

Detrital Zircon Provenance and Lithofacies Associations of Montmorillonitic Sands in the Maastrichtian Ripley Formation: Implications for Mississippi Embayment Paleodrainage Patterns and Paleogeography

Jennifer N. Gifford ^{1,*}, Elizabeth J. Vitale ¹, Brian F. Platt ¹ , David H. Malone ²  and Inoka H. Widanagamage ¹

¹ Department of Geology and Geological Engineering, University of Mississippi, Oxford, MS 38677, USA; ejayvit@gmail.com (E.J.V.); bfplatt@olemiss.edu (B.F.P.); ihwidana@olemiss.edu (I.H.W.)

² Department of Geography, Geology, and the Environment, Illinois State University, Normal, IL 61790, USA; dhmalon@ilstu.edu

* Correspondence: jngiffor@olemiss.edu; Tel.: +1-(662)-915-2079

Received: 17 January 2020; Accepted: 15 February 2020; Published: 22 February 2020



Abstract: We provide new detrital zircon evidence to support a Maastrichtian age for the establishment of the present-day Mississippi River drainage system. Fieldwork conducted in Pontotoc County, Mississippi, targeted two sites containing montmorillonitic sand in the Maastrichtian Ripley Formation. U-Pb detrital zircon (DZ) ages from these sands ($n = 649$) ranged from Mesoarchean (~2870 Ma) to Pennsylvanian (~305 Ma) and contained ~91% Appalachian-derived grains, including Appalachian–Ouachita, Gondwanan Terranes, and Grenville source terranes. Other minor source regions include the Mid-Continent Granite–Rhyolite Province, Yavapai–Mazatzal, Trans-Hudson/Penokean, and Superior. This indicates that sediment sourced from the Appalachian Foreland Basin (with very minor input from a northern or northwestern source) was being routed through the Mississippi Embayment (MSE) in the Maastrichtian. We recognize six lithofacies in the field areas interpreted as barrier island to shelf environments. Statistically significant differences between DZ populations and clay mineralogy from both sites indicate that two distinct fluvial systems emptied into a shared back-barrier setting, which experienced volcanic ash input. The stratigraphic positions of the montmorillonitic sands suggest that these deposits represent some of the youngest Late Cretaceous volcanism in the MSE.

Keywords: detrital zircon geochronology; Mississippi embayment; lithofacies analysis; sedimentology; ichnology

1. Introduction

Time constraints on the initiation of the present-day Mississippi River drainage system have benefitted from recent detrital zircon (DZ) studies that establish its emplacement by the Maastrichtian [1–3]. This has important implications for the paleogeography and tectonic history of North America, particularly in the Mississippi Embayment (MSE), where seismicity continues to the present. Here, we provide new data from the Ripley Formation in northern Mississippi to support Gulf-of-Mexico-directed flow from eastern North America during the Maastrichtian.

The Maastrichtian (72.1 Ma to 66.0 Ma) upper Ripley Formation (Fm) outcrops in Alabama (AL), Mississippi (MS), and Tennessee (TN) [4] and records a period of increased volcanism that is represented by numerous bentonitic intervals (e.g., [4,5]). In Pontotoc County, MS, the purest of these bentonites

were mined in the 1940s by the Mississippi Minerals Company and Eastern Clay Products Inc. Recent investigations within an active sand quarry in central Pontotoc County (Figure 1), yielded a clay-rich interval in the Chiwapa Sandstone Member (CSM) of the Ripley Formation that was confirmed to be montmorillonitic through X-ray diffraction (XRD) by the Mississippi Mineral Resources Institute (MMRI) [6]. The location of the newly discovered montmorillonitic sand is ~10 km south of the 1940s mined bentonite location. In 2018, another expansive clay deposit, exhibiting the field characteristics of smectite-group minerals, was also found above the CSM in northeastern Pontotoc County ~7 km northeast of the 1940s mined bentonites (Figure 1B,C).

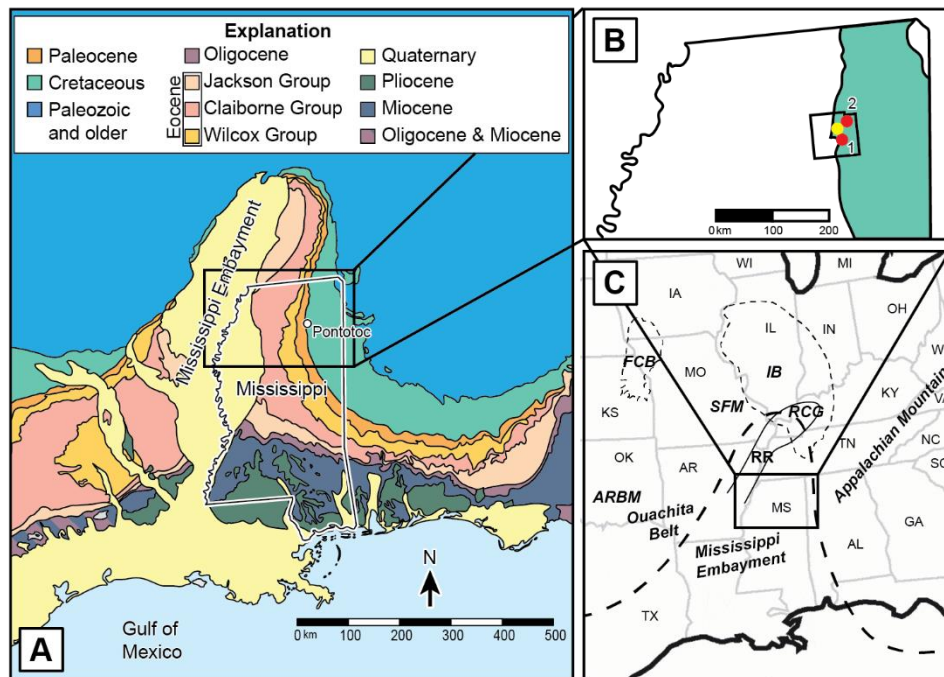


Figure 1. Cretaceous outcrops, basin locations, and structural maps of the Mississippi Embayment and central United States. (A) Mississippi Embayment outcrops with the location of Pontotoc County, MS (modified from Reed et al. [7]). (B) Locations of (1) southern sample location dots and (2) northern sample location are marked by red dots while the previously mined bentonite location is marked by a yellow dot. (C) Basin and structures of the central and eastern United States. ARBM—Arbuckle Mountains; FCB—Forest City Basin; IB—Illinois Basin; RCG—Rough Creek Graben; RR—Reelfoot Rift.

Our initial approach to the project was to determine the age of the ash that weathered to montmorillonite, with a secondary goal of determining DZ provenance to improve interpretations of paleodrainage patterns. We also undertook a lithofacies analysis to interpret the depositional environments of the montmorillonitic sand.

2. Background and Geologic Setting

2.1. Mississippi Embayment Sedimentation

The MSE is a ~259,000 km² south-plunging syncline that extends from southern Illinois (IL) into parts of Alabama (AL), Arkansas (AR), Kentucky (KY), Louisiana (LA), Mississippi (MS), Missouri (MO), Tennessee (TN), and Texas (TX) (Figure 1A,C). The MSE is underlain by the Reelfoot Rift zone, a Neoproterozoic to lower Cambrian aulacogen that formed during the breakup of Rodinia. Despite its age, the Reelfoot Rift zone is currently the most seismically active structural province in the eastern United States [8–10] and it is linked to the New Madrid Seismic Zone, in the northwestern and central MSE. The New Madrid Seismic Zone is characterized by Late Proterozoic to Early Paleozoic

seismogenic faulting [8,10,11] that is still active, as indicated by historical epicenters oriented linearly along the southeastern margin of the Reelfoot Rift [12].

Sediment began accumulating in the Reelfoot Rift basin following early Cambrian rifting, and subsidence roughly kept pace with sedimentation from the late Cambrian to Middle Ordovician [13–15]. From the Middle Ordovician through the Early Cretaceous, terrigenous input waned, allowing carbonate deposition to dominate until the assembly of Pangaea [1,16,17]. During the late Paleozoic, uplift and erosion resulted in an unconformity above upper Paleozoic strata [10]. By the Early Cretaceous, drainage systems extended from the Appalachians to the eastern shoreline of the western interior basin [1,17]. During the Cenozoic, renewed subsidence rerouted terrigenous sediment into the MSE, ultimately resulting in a succession of Mesozoic and Cenozoic rocks and sediments up to 5500 m thick [4].

U-Pb DZ age dating of Cretaceous sediment sources in the MSE have been conducted previously in the Cenomanian Tuscaloosa and Woodbine Fms and Paleocene Wilcox strata [1]. Those data show a pattern of east-to-west and south-to-north continental drainage within the eastern two thirds of North America which dominated through the mid-Cretaceous [1]. Drainage to the Gulf of Mexico (GoM) was restricted to areas in the south. DZ evidence suggests that this continental-scale system drained the north side of the Appalachian–Ouachita chain, crossed the central United States, and routed sediments from eastern and southern North America to the Boreal Sea [1]. Blum and Pecha [1] conclude that the Appalachian-derived transcontinental drainage ended with Late Cretaceous flooding of the Western Interior Seaway and the MSE. Rivers in the southern United States either drained continental arc, Sevier, and Laramide topography into the western GoM in Texas, or merged into the western ancestral Mississippi River and its eastern Appalachian-derived tributaries within the MSE [1]. Blum and Pecha [1] conclude that the reorganization of drainage in the eastern two thirds of Laurentia began in the Jurassic and was completed by the mid-Cretaceous to the Paleocene.

Potter-McIntyre et al. [3] expanded on the work of Blum and Pecha [1] and Blum et al. [2] by determining the U-Pb provenance of the Cretaceous McNairy Formation in southern Illinois. They concluded that the beginning and early evolution of the ancestral Mississippi River initiated with renewed subsidence of the Reelfoot Rift system and the MSE beginning in the Cenomanian, and that the ancestral Mississippi integrated into the Reelfoot Rift/MSE drainage axis by the Maastrichtian [3]. During the Cenomanian, subsidence in the southern Reelfoot Rift/northern MSE began due to the opening of the GoM (e.g., [8,16,18]) and deposition resulted in isostatic subsidence. DZ data from Potter-McIntyre et al. [3] reveal that the sediment was from reworked Pennsylvanian strata that, due to the northern MSE being a topographic high, was exposed in the Cenomanian. As deposition continued, the subsidence of the MSE began to propagate northward, which led to the Paleogene integration of the Ancestral Mississippi River (e.g., [1,2,17,19]). However, Sloss [20] noted that sea level fluctuated during this time, with rapid transgressions followed by slow regressions, and basinward progradation of sediment. The Maastrichtian McNairy Sandstone of Potter-McIntyre et al. [3] was deposited during these transgressive cycles when the MSE had subsided, continuing to create a topographic low allowing the GoM to extend northward, and by the Maastrichtian, was producing fluviodeltaic deposition within the Illinois Basin. Potter-McIntyre et al.'s [3] interpretation of DZs led to the hypothesis that the Mississippi River's south drainage began during the Maastrichtian.

2.2. Ripley Formation Stratigraphy

In Pontotoc County, MS, the Ripley Fm is ~8 to 82 m thick and is dominantly bedded micaceous sand with lenses of silty chalk, chalky limestone, sandy limestones, and bentonite beds that underlie sandy limestones [21]. In this region, it is conformably underlain by the Demopolis Chalk, unconformably overlain by the Owl Creek/Prairie Bluff Fm, and is informally divided into four units (Figure 2). At the base is the “transitional clay”—12 to 15 m of green/gray, well-bedded calcareous sandy clay. Second, is the lower Ripley—9 to 15 m of micaceous calcareous sands and fossiliferous silty limestones. The third unit is the middle Ripley, which is 15 to 46 m thick and divided into three intervals: (1) a lower interval

of micaceous sands with lenses of mixed carbonates and clastics or glauconitic sands, (2) a middle interval containing unfossiliferous sands and lignitic beds, and (3) well-bedded fine-to-medium sands that are similar to the McNairy Sand to the north. Finally, the upper Ripley contains the CSM and the previously mined Pontotoc bentonites [21,22].

Era	Period	Epoch	Age	Ma	Stratigraphic Units
Mesozoic	Cretaceous	Late	Maastrichtian	66	Owl Creek/Prairie Bluff Formation
				Ripley Formation	upper Ripley
					Chiwana Sandstone Member
					middle Ripley
					lower Ripley
Transitional Clay					
Campanian	72.1	Demopolis Chalk			
	Sardis Formation				
	83.6	Coffee Sand			

Figure 2. Generalized stratigraphic column of the Late Cretaceous units of northeastern Mississippi. Modified from Swann and Dew [23], Walker et al. [24], and Dockery [25].

The previously mined bentonites were laterally extensive and pure enough to be considered an economic resource in the 1940s [21,22]. The bentonite outcrops described by Priddy [21] were based on a coarse sand located either within or above the CSM, which graded into a less silty, less calcareous clay that then graded into a dark blue/gray, silty, calcareous clay. The bentonite reached a maximum thickness of ~2.7 m in northern Pontotoc County and thinned to ~0.6 m in the southeast [22]. The lack of exposed bentonites within the entire upper Ripley was interpreted as the result of erosion before deposition of the uppermost upper Ripley member [21].

3. Methods

3.1. Sample Collection and Preparation

Samples were collected at the two locations where expansive clay was observed in Pontotoc County, MS (Figure 1B). The northern site is in northeast Pontotoc County, off Tuscumbia Road (34.34917°N, 88.90722°W) (Figure 1B). The southern site is in a sand quarry southeast of the city of Pontotoc (Figure 1B), near state highway 41 (34.20417°N, 88.97778°W). The outcrop is ~9 m below the K–Pg boundary, determined by pacing and correcting for slope. The two sites are ~17.4 km apart from each other as the crow flies.

Samples from the southern site were collected from two trenches that were excavated ~15 m apart, one to the northeast (NE) and one to the southeast (SE) in a weathered high wall from previous sand mining within the upper Ripley (Figure 1B). Detailed stratigraphic sections were measured and lithofacies were characterized at each location. Bulk samples at the southern location were collected in ~1 m intervals with additional samples collected from the expansive clay-rich interval. Northern samples were collected from sections exposed by previous mining activity (Figure 1B).

Samples were oven dried and pulverized in the University of Mississippi Geochronology laboratory using a disk mill. The southern site zircons were initially separated using a centrifugal bowl that separated sediment based on grain density and slightly on grain size as finer particles were washed

out of the sample in addition to lighter density particles. The northern site samples were separated using a Jasper Canyon Research (JCR) zircon-concentrating table. After washing, the heavy fractions were gathered and dried before undergoing heavy liquid separation. Lithium Polytungstates (LST; specific gravity (SG) = ~ 2.85) were used to separate lighter minerals from the heavy fraction based on density and were then run through a magnetic separator (Franz LB-1). The non-magnetic fraction was separated with methylene iodide (MI) (SG = ~ 3.30) to yield zircon grains.

Zircon grains were handpicked under a microscope and > 120 grains per sample were mounted on a glass plate using adhesive tape. The selected zircon grains were embedded in a 2.54 cm diameter epoxy plug and polished for imaging approximately halfway through the zircon grains.

3.2. Scanning Electron Microscope Imaging

Zircons were imaged at the Mississippi State University Institute for Imaging and Analytical Techniques (I²AT) using a Zeiss EVO 5.0 high-vacuum Scanning Electron Microscope (SEM) and a Gatan miniCL cathodoluminescence attachment. Secondary Electron (SE) and cathodoluminescence (CL) images were collected and used to characterize grain zoning and classification (igneous, metamorphic, or detrital) (Figure 3). Targets for U–Pb laser ablation ($\sim 20 \mu\text{m}$) were selected on the CL images for each grain based on zonation. Some grains had multiple U–Pb sites based on the presence of a core and rim in the same grain that could possibly yield different ages.

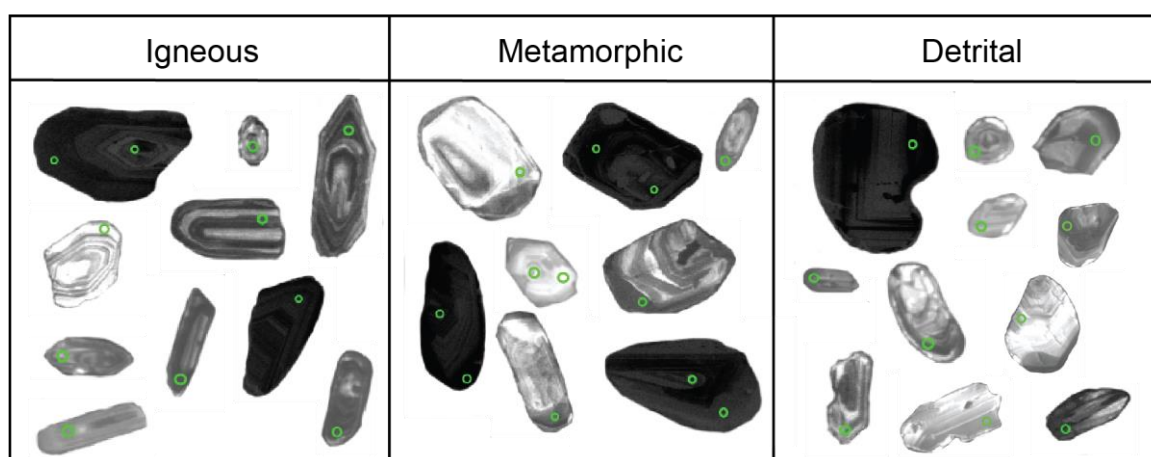


Figure 3. A range of detrital zircon morphologies and the zonation CL images grains from all 11 samples. The $\sim 20 \mu\text{m}$ laser ablation spots are indicated by circles on the individual grains.

3.3. Uranium–Lead (U–Pb) Zircon Isotopic Analysis

U–Pb analyses for the initial samples from the southern site (SE140 and NE100) were performed on a Nu Plasma 3-D Multi-collector inductively coupled plasma-mass spectrometer (Nu-ICP-MS) at the University of Florida Department of Geosciences, Geochronology Laboratory. Zircon ablation occurs in a stream of He and is then mixed into an Ar gas flow that carries minute particles of zircon into the plasma stream, which ionizes them, allowing U and Pb isotopes to be measured simultaneously using the multi-collector. Ion collectors on the end of the Nu-ICP-MS simultaneously collect ^{204}Pb (^{204}Hg), ^{206}Pb , and ^{207}Pb ions and Faraday detectors collect ^{235}U and ^{238}U signals. A 20-s integration that clears the gas blank and the ^{204}Hg input precedes a 30-s period that clears the previous analysis. After the completion of Nu-ICP-MS analysis, isotopic ratios of $^{206}\text{Pb}/^{238}\text{U}$, $^{207}\text{Pb}/^{235}\text{U}$, and $^{207}\text{Pb}/^{206}\text{Pb}$ were provided from the Nu-Instruments Time Resolved Analysis software. To correct the fractionation and drift errors that occurred, corrections were calibrated against a known standard (FC-1 natural zircon standard; Duluth Gabbro; 1098 Ma; [26,27]). Analyses were arranged with 2 ablations of FC-1, followed by 10 unknowns, and then 2 more FC-1. Collected data were input into the CALAMARI 9.0 (© P. Mueller) reduction protocol for U–Pb geochronology spreadsheet.

GeoSep Services (GSS) in Idaho analyzed the sample TR-02 from the northern site. Isotopic analyses used a New Wave UP-213 laser ablation system along with an Agilent 7700x quadrupole inductively coupled plasma-mass spectrometer (LA-ICP-MS) at the Washington State University GeoAnalytical Lab. Material was delivered to the plasma source by a stream of He and Ar gas. Each analysis cycle took ~30 s and consisted of a 6-s integration with the laser shutter closed to collect background measurements followed by a 24-s integration with the laser shutter open. Analyses were separated by a 20-s delay and measured the following isotopes: ^{202}Hg , $^{204}(\text{Hg} + \text{Pb})$, ^{206}Pb , ^{207}Pb , ^{208}Pb , ^{232}Th , ^{235}U , and ^{238}U . U–Pb age standards were used during analysis for calibration purposes. Laser ablations consisted of 2 ablations of the FC-1 standard, 10 ablations of the zircon sample, and 2 more FC-1 ablations [26]. FC-1 was used in order to correct the fractionation and drift errors that occurred, corrections were then calibrated against a known standard [26,27]. Collected analytical data were input into the GSS-ZrnUPb (© Geoseps Services, LLC) reduction protocol for U–Pb geochronology spreadsheet.

All remaining samples were analyzed by laser ablation ICP-MS using a Varian 810 Quadrupole ICP-MS coupled with a PhotonMachines Analyte.193 excimer laser at the University of Arkansas Trace Element and Radiogenic Isotope Lab. Data reduction methods are outlined in Shaulis et al. [28]. Laser ablations consisted of 2 ablations of the FC-1 and Plešovic standard, 15 ablations of the zircon sample, and 2 more FC-1 and Plešovic ablations [26,29]. Concentrations of U and Th are calibrated relative to the NIST612 standard zircon, which contains ~765 ppm of U and 80 ppm Th.

U–Pb analyses were sorted based on discordance, and those between $< 10\%$ or $> -5\%$ reversely discordant were approved for inclusion in the final dataset. These discordance thresholds are arbitrary, but are a widely accepted range to remove damaged grains from the data set (e.g., major Pb loss or large amounts of common Pb). After sorting based on discordance, analyses were chosen for each sample. For ages < 800 Ma, $^{206}\text{Pb}/^{238}\text{U}$ ages are used and for grain ages > 800 Ma, $^{207}\text{Pb}/^{206}\text{Pb}$ ages are used. These ages were used to create probability density plots (PDPs) in Isoplot 3.75 [30] which show the number and relative probability of the grain ages along with the potential source locations. Cumulative age-probability plots (CDPs) were created using the analytical spreadsheet created by the Arizona Laserchron Center [31] and are a visual tool used to show the cumulative age data by graphically comparing the cumulative probability for each sample on a single graph.

3.4. Statistical Analysis

Statistical analyses were performed in order to compare samples using Kolmogorov–Smirnov (K–S) tests [32] and Multidimensional Scaling (MDS). K–S tests were performed using the analytical spreadsheet from the Arizona Laserchron Center [32]. The K–S test compares and differentiates the DZ age spectra and tests the null hypothesis that the samples are from the same population based on a $> 95\%$ confidence level, represented by the p -value [32]. These tests are based on the cumulative density functions (CDFs) that create the CDPs [31]. The K–S test compares the maximum vertical probability distances between the curves and a value based on the number of samples in the distribution and confidence level, which is referred to as the critical value [32]. If the distance between two sample CDFs is greater than the critical value, then the null hypothesis is rejected, and DZ samples did not originate from the same source ($p < 0.05$). Therefore, the K–S test only indicates if populations are statistically different rather than whether the populations are the same [33], and if the p -value is greater than 0.05, then the two DZ age spectra may share the same provenance.

The K–S test is not without its criticisms. p -values may be strongly dependent on sample size, which can sometimes limit their usefulness for detrital geochronology [34]. The K–S statistic can be considered less sensitive at the extreme ends of the distributions [35], and it can be biased by near-unimodal distributions. However, Vermeesch [36] argued that it is more reliable in distinguishing provenance similarities than other dissimilarity statistics. Lower K–S values suggest relatively low distribution dissimilarities and may be used as support for common source regions. This statistical technique provides quantitative support for visual curve matching.

To overcome the potential limitations of our K–S tests, we supplemented our analyses with non-metric MDS using K–S dissimilarity in the package *provenance* for R [37]. MDS generates a matrix of D statistics—the maximum differences between successive pairs of cumulative density functions—calculated as part of the K–S test. The matrix is used to graphically represent relative dissimilarities in Euclidean space, where each DZ population plots as a point and the distance between points represents their dissimilarity values, i.e., samples with high similarities plot near each other, and samples that are highly dissimilar plot further apart [34]. MDS has been used relatively recently to compare DZ datasets (e.g., [36,38–42]) and it has proven to be particularly useful when visualizing the dissimilarity of a large set of samples [34,38,39]. Following the recommendation of Vermeesch [36], we include solid and dotted lines connecting points on our MDS plot to represent the least dissimilar and second least dissimilar samples, respectively [34,36].

K–S tests were performed to compare all of the samples at the southern location to each other as well as all of the samples at the northern location to each other (MDS was not used in these cases because of the small sample sizes). The cumulative southern and cumulative northern data sets were then compared using a K–S test and MDS. Finally, a K–S test and MDS were used to compare the Pontotoc samples to strata with hypothesized shared provenance: Cenomanian strata and modern sediments from the GoM [1], Cretaceous sands in the Forest City Basin (FCB), Iowa [17], the Mesoproterozoic Mid-Continent Rift [43], the Paleozoic Mid-Continent [44], strata in the Illinois Basin [3,45], Paleozoic strata in the Black Warrior Basin [46,47], and Appalachian Foreland Basin strata [48–50]. The K–S results are provided in the Supplementary Material.

3.5. X-ray Diffraction (XRD) Analysis

To identify expansive clay mineralogy, two samples were collected from each apparent bentonitic interval from the northern and southern Pontotoc sites for XRD analysis. All four samples were powdered in house at the University of Mississippi and then sent to Mississippi State for analysis. XRD analysis was performed at the I²AT using a Rigaku Ultima III X-ray Diffraction System. Please note that bentonites are defined as clay deposits dominated by smectite-group minerals, commonly montmorillonite, formed from alteration of volcanic ash [51]. For our purposes, the presence of any smectite-group minerals would be significant as indicators of Maastrichtian volcanism in the region, regardless of whether the targeted units can be classified as true bentonites.

4. Results

4.1. Lithofacies

We recognize six lithofacies in the field areas. Because of the friable and erosive nature of the material, exposures are limited and lateral lithofacies variations and relationships cannot always be evaluated. The stratigraphic relationships between lithofacies are represented in Figure 4.

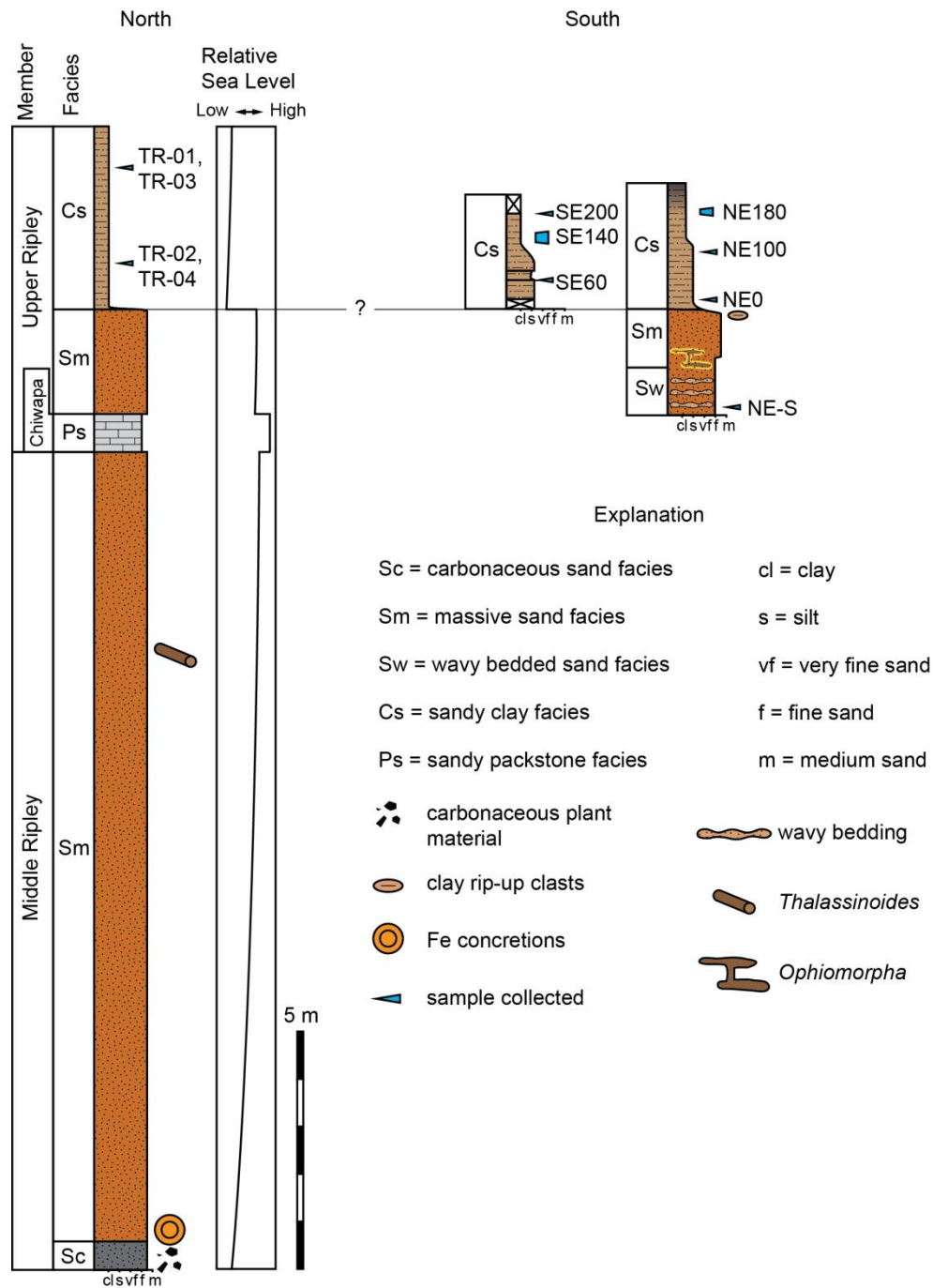


Figure 4. Stratigraphic sections measured at the northern and southern sites, including sample collection locations, lithofacies designations, and interpreted relative sea-level curve.

4.1.1. Sandy Clay Lithofacies

Very thickly bedded (180–385 cm), massive, poorly sorted, sandy gray to red clay with matrix-supported, very fine to coarse, but dominantly medium-sand-sized, subangular to subrounded quartz grains with rare very-fine-sand-sized muscovite grains and local concentrations of clay, some as mm-scale diameter spherical aggregates that spall out of freshly exposed surfaces (Figures 4 and 5A). Beds fine upward to silty clay and contain somewhat laterally extensive (traceable for tens of meters) lenses of less sandy gray clay with irregular boundaries, as if disrupted by bioturbation (Figures 4 and 5B,C). This lithofacies weathers to sloped surfaces with polygonal desiccation cracked patterns when dry (Figures 4 and 5D), which led us to hypothesize that this lithofacies contained expansive clays. The upper ~145 cm of the

beds show angular blocky and wedge ped structure, black ped coatings, and abundant grass roots, representing recent soil development at the modern surface. Spherical clay aggregates are found below the zone of soil development.

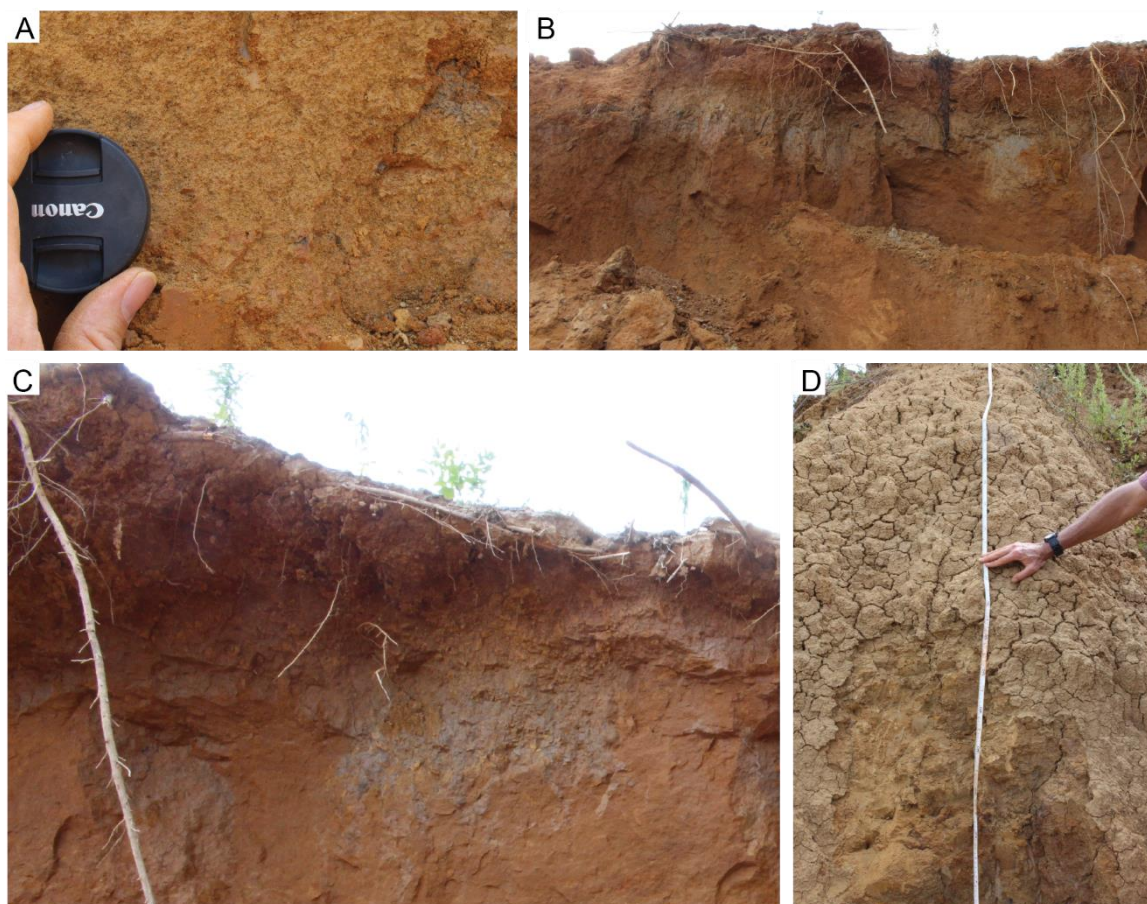


Figure 5. Sandy clay lithofacies. (A) Spherical clay aggregates in outcrop at the southern Pontotoc site. Lens cap is 5.5 cm in diameter. (B) Gray lens of sandy clay lithofacies exposed in high wall of quarry at southern site. Lens is ~0.5 m thick. (C) Portion of lens in B showing diffuse lower boundary possibly from bioturbation. (D) Cracked surface weathering pattern indicating the presence of expansive clays. Tape measure is marked in cm.

4.1.2. Carbonaceous Sand Lithofacies

The complete thickness of this lithofacies could not be observed because it is present at the base of the measured section and is not fully exposed. Beds are at least 60 cm thick and consist of mostly massive, poorly sorted, fine-to-medium, subrounded to subangular quartz sand grains within a dark gray clay matrix (Figures 4 and 6A) with sporadic, thin, discontinuous beds of organic-rich sand and sporadic, irregularly shaped lenses of white sand with orange rims, possibly representing bioturbation. Also present are undulatory, thick lamina of resistant iron cemented sandstone. There is an upward decrease in clay content and the uppermost bounding surface is sharp, undulatory, and marked by a layer of resistant Fe-cemented sandstone (Figures 4 and 6B).



Figure 6. Sand and limestone lithofacies. (A) Sharp contact between carbonaceous sand lithofacies and massive sand lithofacies. Jacob staff marked in dm. (B) Fe-rich concretion at contact between carbonaceous sand and massive sand lithofacies. Scale is in cm. (C) Wavy-bedded sand lithofacies. 5.5 cm diameter lens cap for scale. (D) Massive sand lithofacies overlying carbonaceous sand lithofacies. Note resistant layers of Fe-cemented sand. Rock hammer is 32 cm long. (E) *Ophiomorpha* in the massive sand lithofacies at the southern site. Hand for scale. (F) *Thalassinoides* in the massive sand lithofacies at the northern site. Note concentric laminae (ovals). Lens cap is 5.5 cm in diameter. (G) Ripple-laminated sand lithofacies. Dashed lines highlight slump planes. Lens cap is 5.5 cm in diameter. (H) Sandy packstone lithofacies at northern site. Size 12 boot for scale.

4.1.3. Wavy-Bedded Sand Lithofacies

Very thickly bedded (> 200 cm), poorly sorted, orange-brown, silty fine sand that is dominantly subangular to subrounded quartz grains. Wavy bedding is the dominant sedimentary structure (Figures 4 and 6C), with rare lenticular bedding. Wavy bedding consists of poorly sorted (mud-rich), slightly darker sand interbedded with better-sorted, slightly lighter colored sand. No body fossils or trace fossils were observed. Lower boundaries of this lithofacies were not observable in the field, but upper contacts were gradational into the massive sand lithofacies.

4.1.4. Massive Sand Lithofacies

Very thickly bedded (220 to 1660 cm), massive, tan to orange, friable, poorly sorted, fine-to-medium, dominantly quartz, subangular to subrounded sand. Gray to white clay is present as matrix and as local resistant lenses, laminae, thin beds, and rare rip-up clasts. Iron-oxide-cemented thin beds, thick laminae, and concretions with concentric fabric are present towards the bases of beds, particularly at the sharp, undulatory basal contact with the carbonaceous sand lithofacies (Figures 4 and 6D). Basal contacts are gradational where underlain by the wavy-bedded sand lithofacies. Upper contacts are sharp where overlain by the sandy packstone lithofacies and gradational where overlain by the sandy clay lithofacies. Neither organic matter nor body fossils were observed.

Two types of trace fossils are abundant in localized horizons. Type 1 traces (Figures 4 and 6E) are exposed only in two dimensions on trench walls, but consist of horizontal to subhorizontal and vertical shafts that intersect. Shafts are up to ~ 3 cm wide and are walled by 0.5 to 1 cm thick yellow mud and sand that appear smooth to pellet-like and resistant. Shaft fill is brown sand that is darker and coarser than the surrounding matrix. Shaft diameters vary along their lengths and some appear to contain rounded enlargements. Type 2 traces (Figures 4 and 6F) are horizontal, subhorizontal, and subvertical, resistant, cylindrical tubes of consistent diameter that range from 1 to 3 cm in diameter. Only short segments of the tubes are exposed so it is unknown whether they intersect. Tubes are walled with < 0.5 cm thick walls, some of which have iron oxide cement. Fill is concentric laminae of mud and fine sand, some white and some the same color as the matrix. The two types of trace fossils are not found together in the same horizons.

4.1.5. Ripple-Laminated Sand Lithofacies

Thick bedded (up to 50 cm), friable, ripple-laminated, light brown, poorly sorted, fine-to-medium, subrounded to subangular quartz sand (Figures 4 and 6G). Ripple lamination is subtle and difficult to see without proper lighting. Ripples are asymmetrical, but postdepositional slumping and microfaulting make it difficult to determine current direction. This lithofacies grades upward into the sandy clay lithofacies and grades laterally into the wavy-bedded sand lithofacies. No fossils were observed.

4.1.6. Sandy Packstone Lithofacies

Thickly bedded (~80 cm), tan to gray, resistant, highly fossiliferous limestone with sand-rich matrix (packstone) (Figures 4 and 6H). No sedimentary structures were observed. Whole and fragmented fossils present include bivalves (including *Exogyra*), cephalopods (including the ammonite *Sphenodiscus* and belemnites), echinoids (including *Hardouinia*), decapod crustaceans, gastropods, and shark teeth. Possible burrow casts were also present.

4.2. Zircon Geochronology

DZ provenance studies are possible because DZ ages correspond to crystallization ages of the individual cratonic elements that amalgamated over billions of years to form the continents in their current configurations [52]. Figure 7 details the identified igneous provinces of North America which are broken down into the following sections: Superior Province (> 2500 Ma), Trans-Hudson/Penokean (1900–1800 Ma; T-H/P), Yavapi–Mazatzal (1800–1600 Ma; Y–M), Mid-Century Granite–Rhyolite

province (1600–1350 Ma; MCGRP), Grenville (1350–900 Ma), Gondwanan Terranes (900–500 Ma), Taconic (490–440 Ma), Acadian (450–320 Ma), and Alleghanian (330–265 Ma). A detailed discussion of the North American igneous terranes with related citations can be found in Appendix A.

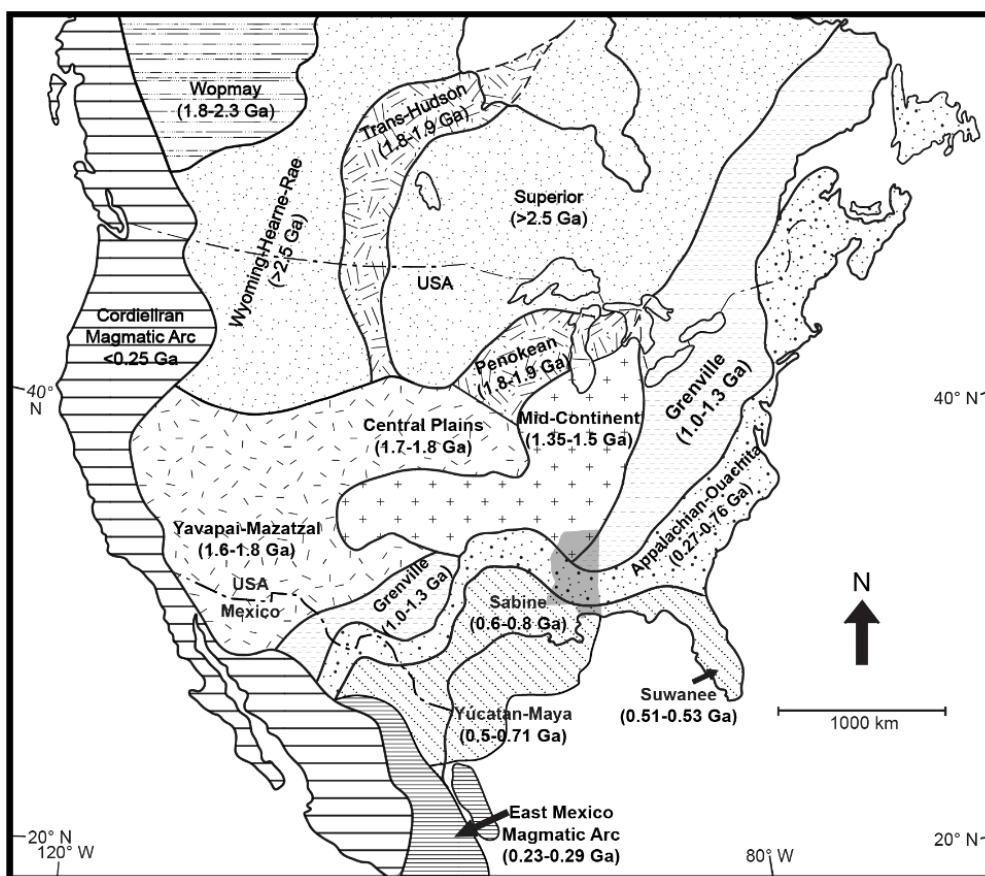


Figure 7. Igneous provinces of North America. Modified from Dickinson and Gehrels [53] and Alsalem et al. [54].

A total of 649 U–Pb analyses were collected that fit the criteria across 11 samples (Figure 8). Age analysis shows an overall age range of 2870 Ma to 305 Ma. All U–Pb analyses are available in the Supplementary Materials (Table S1). The potential source age range percentages for the southern and northern samples are summarized in Table 1.

Table 1. North American igneous province age distribution and percentages for the northern sample population (NS) and southern sample population (SS).

North American Age Provinces	Northern Samples	Southern Samples	Combined
	n = 273	n = 376	n = 649
Alleghanian (330–265 Ma)	0.0%	1.1%	0.6%
Acadian (450–320 Ma)	1.8%	10.6%	6.9%
Taconic (490–440 Ma)	3.3%	0.3%	1.5%
Gondwanan Terranes (900–500 Ma)	1.1%	2.9%	2.2%
Grenville (1350–900 Ma)	80.2%	80.1%	80.1%
MC-Granite-Rhyolite (1600–1350 Ma)	9.9%	4.5%	6.8%
Yavapai–Mazatzal (1800–1600 Ma)	1.5%	0.0%	0.6%
Trans-Hudson/Penokean (1900–1800 Ma)	0.7%	0.0%	0.3%
Superior Province (> 2500 Ma)	1.5%	0.5%	0.9%

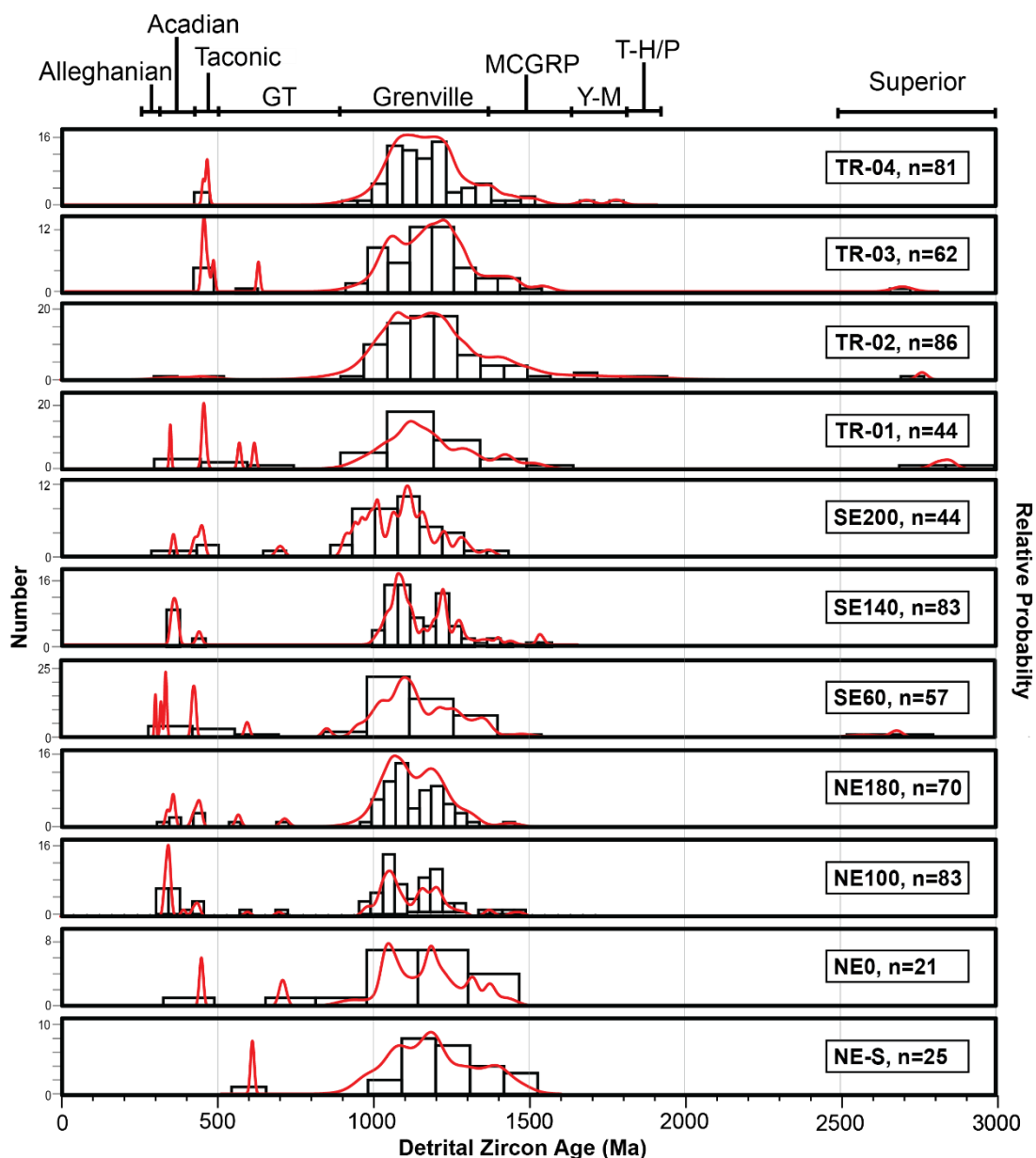


Figure 8. Stacked age-probability density plots of the 11 northern and southern samples.

4.2.1. U–Pb Geochronology of Southern Samples

The seven southern samples ($n = 376$) have detrital age spectra of mostly Grenville-aged grains (80.1%, $n = 301$) (Figure 9). Acadian-aged grains make up the next dominant group with 10.6% of the grains ($n = 40$) coming from the 450–320 Ma age range. The remainder of the age groups, in descending order, are: MCGR (4.5%, $n = 17$), Gondwanan Terranes (2.9%, $n = 11$), Alleghanian (1.1%, $n = 4$), Superior (0.5%, $n = 2$), and Taconic (0.3%, $n = 1$) (Figure 9). The southern samples did not yield any results from the Yavapai–Mazatzal or Trans-Hudson/Penokean provinces (Table 1; Figure 9). Although detailed sample descriptions of sample separates were not recorded, heavy mineral separation yielded high amounts of kyanite within the southern samples.

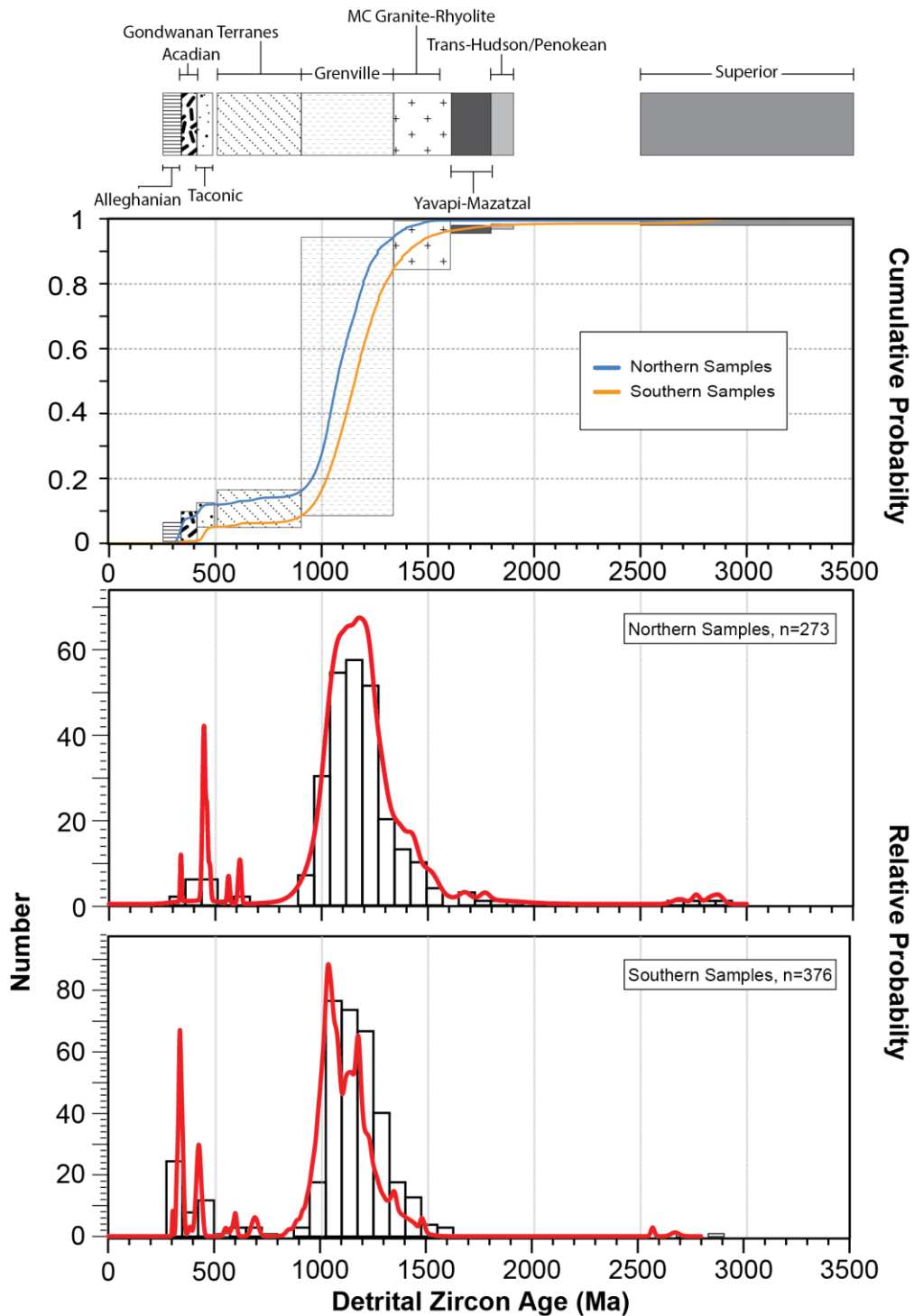


Figure 9. Stacked cumulative and normalized Age-probability density plots of the NS and SS.

Sample NE-S. This sample was collected from the wavy-bedded sand lithofacies (Figure 4). U–Pb zircon analyses ($n = 25$) for this sample range in age from 1372 Ma to 602 Ma. The PDP for sample NE-S contains a dominant double peak at ~1172 Ma and ~1081 Ma in the Grenville age range along with two other age peaks at ~602 Ma (Gondwanan Terranes) and ~1386 Ma (MCGRP) (Figure 8).

Sample NE0. This sample was collected at the base of the sandy clay lithofacies in the northeastern trench (Figure 4). U–Pb zircon analyses ($n = 21$) for this sample range in age from 1400 Ma to 440 Ma. The PDP for sample NE0 has a dominant double peak at ~1167 Ma and ~1036 Ma in the Grenville

age range along with two other age peaks at ~444 Ma (Taconic) and ~698 Ma (Gondwanan Terranes) (Figure 8).

Sample NE100. This sample was collected from the middle of the sandy clay lithofacies within the northeastern trench (Figure 4). U–Pb zircon analyses ($n = 76$) for this sample range in age from 1447 Ma to 326 Ma. The PDP for sample NE100 has a dominant double peak at ~1176 Ma and ~1033 Ma in the Grenville age range along with two other age peaks at ~337 Ma (Alleghanian) and ~428 Ma (Taconic/Acadian). Minor age occurrences also appear in the Gondwanan Terranes and MCGRP ranges (Figure 8).

Sample NE180. This sample was collected from the sandy clay lithofacies near the top of the northeastern trench (Figure 4). U–Pb zircon analyses ($n = 70$) for this sample range in age from 1410 Ma to 332 Ma. The PDP for sample NE180 has a dominant double peak at ~1163 Ma and ~1041 Ma in the Grenville age range along with two other age peaks at ~357 Ma (Acadian) and ~432 Ma (Taconic/Acadian). Minor age occurrences are present in the Gondwanan Terranes and MCGRP ranges (Figure 8).

Sample SE60. This sample was collected from the lower third of the sandy clay lithofacies (Figure 4). U–Pb zircon analyses ($n = 57$) for this sample range in age from 2667 Ma to 305 Ma. The PDP for sample SE60 has a dominant double peak at ~1110 Ma and ~1222 Ma in the Grenville age range along with three other age peaks at ~337 Ma (Alleghanian) and ~428 Ma (Taconic/Acadian), and ~599 Ma (Gondwanan Terranes). Sample SE60 does show a minor age occurrence in the Superior age range (> 2500 Ma) (Figure 8).

Sample SE140. This sample was collected from the sandy clay lithofacies in the middle portion of the southeastern trench (Figure 4). U–Pb zircon analyses ($n = 83$) for this sample range from 1489 Ma to 333 Ma. The PDP for sample SE140 has a dominant double peak at ~1040 Ma and ~1182 Ma in the Grenville age range along with three other age peaks at ~342 Ma (Alleghanian/Acadian) and ~418 Ma (Acadian), and ~1485 Ma (MCGRP) (Figure 8).

Sample SE200. This sample was collected from the top of the sandy clay lithofacies close to the base of modern soil overprinting (Figure 4). U–Pb zircon analyses ($n = 44$) for this sample range from 1337 Ma to 349 Ma. The PDP for sample SE200 has a dominant double peak at ~1040 Ma and ~1182 Ma in the Grenville age range along with three other age peaks at ~350 Ma (Acadian) and ~435 Ma (Acadian/Taconic), and ~680 Ma (Gondwanan Terranes) (Figure 8).

4.2.2. U–Pb Geochronology of Northern Samples

The combined northern samples are dominantly Grenville in age (80.2%, $n = 219$). The next highest percentage of analyses is the MCGRP at 9.9% ($n = 27$) of the analyses. The remainder of the analyses in descending order are: Taconic (3.3%, $n = 9$), Acadian (1.8%, $n = 5$), Superior (1.5%, $n = 4$), Yavapai–Mazatzal (1.5%, $n = 4$), Gondwanan Terranes (1.1%, $n = 3$), and Trans-Hudson/Penokean (0.7%, $n = 2$) (Figure 10). There were no analyses that were of Alleghanian age (Table 1; Figure 9).

Sample TR-01. U–Pb zircon analyses ($n = 44$) for this sample range in age from 2870 Ma to 338 Ma. The PDP for sample TR-01 has a large Grenville peak at ~1115 Ma along but does not exhibit the standard Grenville double peak. Four large age peaks occur at ages less than Grenville, which differs from the other samples. The four peaks are at ~338 Ma (Acadian), ~446 Ma (Taconic), ~561 Ma, and ~612 Ma, which are both Gondwanan in age. Sample TR-01 does show a minor age occurrence in the Superior age range (> 2500 Ma) and contains the oldest grain found out of all 11 samples (Figure 8).

Sample TR-02. U–Pb zircon analyses ($n = 86$) for this sample range in age from 2762 Ma to 354 Ma. The PDP for sample TR-02 has a dominant double peak at ~1086 Ma and ~1188 Ma along with two peaks at ~449 Ma (Taconic) and ~2754 Ma (Superior) (Figure 8).

Sample TR-03. U–Pb zircon analyses ($n = 62$) for this sample range in age from 2684 Ma to 439 Ma. The PDP for sample TR-03 has a dominant double peak at ~1057 Ma and ~1219 Ma along with two peaks at ~444 Ma (Taconic) and ~618 Ma (Gondwanan Terranes). Sample TR-03 does show a minor age occurrence in the Superior age range (> 2500 Ma) and contains grains in the MCGRP age range (Figure 8).

Sample TR-04. U–Pb zircon analyses ($n = 81$) for this sample range in age from 1769 Ma to 448 Ma. The PDP for sample TR-03 has a subtle double peak at ~ 1105 Ma and ~ 1180 Ma along with an age peak at ~ 461 Ma (Taconic) and contains grains in the MCGR age range (Figure 8).

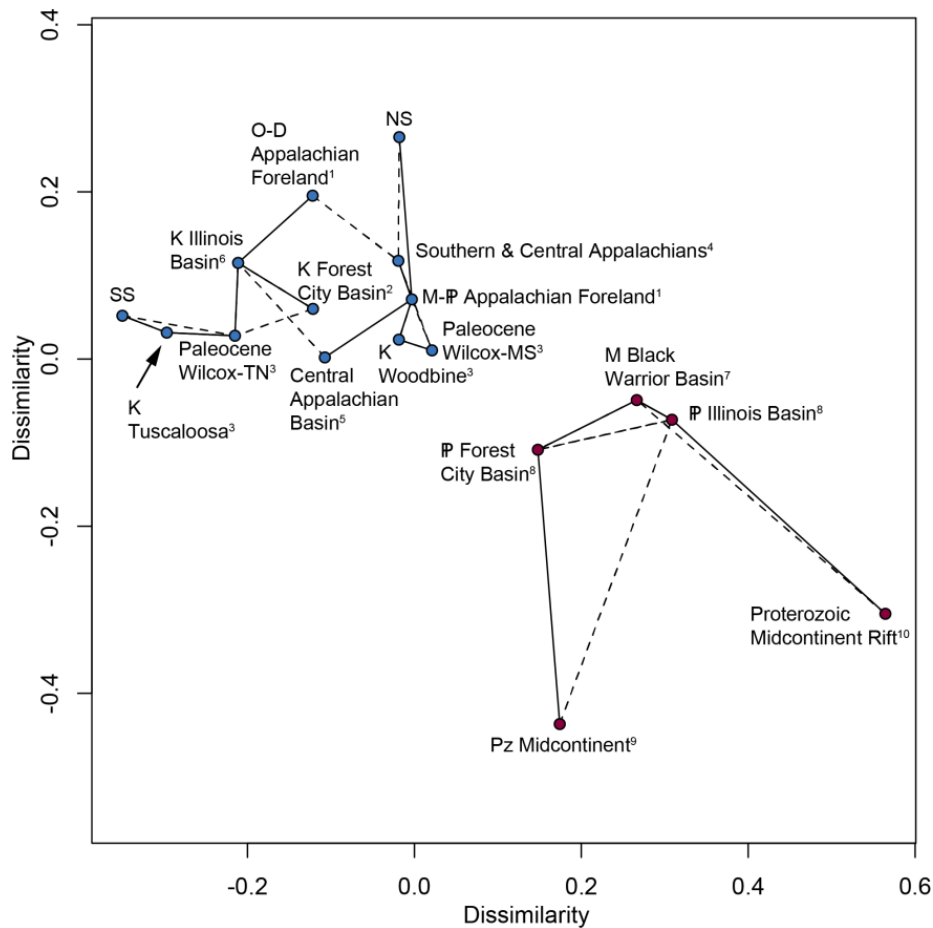


Figure 10. MDS plot representing the dissimilarities between Pontotoc samples and published DZ datasets, solid lines represent pairs of samples with the lowest dissimilarity, dashed lines represent pairs of samples with the second lowest dissimilarity. Please note that sample plot in two groups color coded with blue dots and red dots. SS: Southern sample; NS: Northern sample; O-D Appalachian Foreland: Ordovician and Devonian strata ¹ [50]; M-P Appalachian Foreland: Mississippian–Permian strata ¹ [50]; K Forest City Basin: Cenomanian–Albian Dakota Fm ² [17]; Paleocene Wilcox-TN: strata from Tennessee ³ [1]; Paleocene Wilcox-MS: strata from Mississippi ³ [1]; K Tuscaloosa: Cenomanian Sandstone ³ [1]; K Woodbine: Cenomanian Fm ³ [1]; Southern and Central Appalachians: Paleozoic to Mesozoic strata ⁴ [48]; Central Appalachian Basin: Paleozoic to Mesozoic strata ⁵ [49]; K Illinois Basin: Cretaceous strata ⁶ [3]; M Black Warrior Basin: Mississippian to Pennsylvanian strata ⁷ [46,47]; P Illinois Basin: Pennsylvanian ⁸ [45]; P Forest City Basin ⁸ [45]; Pz Mid-Continent: Cambrian to Ordovician strata ⁹ [44]; Proterozoic Mid-Continent Rift: ¹⁰ [43].

4.3. Statistical Results

The K–S statistical analysis of the seven samples from the southern Pontotoc site yielded p -values > 0.05 (~ 0.06 – 1.0), thus, we accept the null hypothesis that the DZ age spectra are from the same population. The K–S analysis of the four samples from northern Pontotoc likewise yielded p -values > 0.05 (~ 0.6 – 1.0) that indicated that the DZ age spectra are statistically similar. Due to the statistical similarity, the seven southern samples were combined into one southern sample (SS) and the four northern samples were combined into one northern sample (NS). These DZ spectra were then compared

to each other with a K–S test, which yielded a p -value of ~ 0.0000041 indicating that the two datasets are not statistically similar to one another. The K–S statistical analysis of the detrital age spectra for the NS and the Albian–Cenomanian Dakota Fm of Finzel [17] and the Ordovician to Devonian strata of the Appalachian Foreland Basin (AFB) of Thomas et al. [50] are statistically similar ($p = 0.09$ and 0.05 respectively). The SS was found to be statistically similar ($p = 0.66$ and 0.16 respectively) to the Cenomanian Tuscaloosa Fm and the Paleocene Wilcox in Tennessee of Blum and Pecha [1]. Both the NS and SS are statistically distinct from all other Precambrian and Paleozoic strata in the mid-continent [43,44], the other Paleozoic sandstones in the Illinois and FCB [45], the Paleozoic Black Warrior Basin strata [46,47], the Cenomanian Woodbine sandstone [1], and the Paleocene Wilcox Group in Mississippi [1].

The MDS plot (Figure 10) shows two groups: 1) All Pontotoc samples + Paleozoic AFB [48] and Central Appalachian Basin [49] + Cretaceous Forest City Basin [17] + Cretaceous Illinois Basin [3] + Cretaceous–Paleogene GoM coastal plain [1]; and 2) Proterozoic Mid-Continent Rift [43] + Paleozoic Mid-Continent [44] + Mississippian Black Warrior Basin [46,47] + Pennsylvanian Forest City Basin [45] + Pennsylvanian Illinois Basin [45]. The SS is nearest neighbor (least dissimilar) to the Cenomanian Tuscaloosa Formation [1] and second nearest neighbor to the Paleocene Wilcox Group of Tennessee [1]. The NS is nearest to the Mississippian to Pennsylvanian deposits of the AFB [50] and second nearest to the southern and central AFB samples [48].

4.4. XRD Results

XRD results reveal that a large percentage of the northern and southern samples are quartz with other minor minerals (Table 2). The northern samples (TR-01 and TR-04) have a range of 56.9%–49.8% quartz and a high kaolinite presence ranging from 21.9%–17.2% (Table 2). Low amounts of expansive clays such as montmorillonite were measured in these samples (6.2%–3.6%) (Table 2). The southern samples contain 36.6%–46.0% quartz and several constituents with and without expansive properties, including montmorillonite and illite, respectively. The southern samples contain a much lower amount of kaolinite than the northern samples (Table 2). The XRD analysis images are compiled in the Supplementary Files.

Table 2. X-ray Diffraction analysis for two northern samples (TR-01 and TR-04) and two southern samples (Pontotoc-1 and Pontotoc-2).

Northern Location XRD Analysis			
TR-01		TR-04	
Constituent	Weight %	Constituent	Weight %
Quartz	49.8	Quartz	56.9
Kaolinite	21.9	Kaolinite	17.2
Muscovite	13.9	Illite	10
Illite	10.8	Muscovite	9.7
Montmorillonite (Ca, Na rich)	3.6	Montmorillonite (Ca, Na rich)	6.2
Southern Location XRD Analysis			
Pontotoc-1		Pontotoc-2	
Constituent	Weight %	Constituent	Weight %
Quartz	39.9	Quartz	46
Montmorillonite (Na rich)	15.5	Muscovite	16.5
Muscovite	14.1	Kaolinite	16.4
Illite	12.3	Illite	10.4
Kaolinite	9	Montmorillonite (Ca, Na rich)	7.8
Montmorillonite (Ca, Na rich)	4.9	Birnessite	2.9
Birnessite	4.1		

5. Discussion

5.1. Lithofacies Interpretations

5.1.1. Sandy Clay Lithofacies

Clay-matrix supported sand grains represent a relatively low energy environment, while the subangular to subrounded quartz sand, muscovite, and presence of likely volcanic montmorillonite indicate proximity to a terrestrial source. The spherical clay aggregates are found below the zone of soil development and therefore are not pedogenic in origin. The variety of diameters and apparent lack of organic matter argue against a fecal pellet origin. The aggregates are most similar to flocculated clay balls reported from possibly turbulent, brackish water conditions [55]. XRD and SEM analyses of these aggregates may reveal more detailed evidence about their origin, but such analyses are beyond the scope of this paper. Given the sedimentological evidence, this lithofacies may represent an estuary or back-barrier setting. We favor an interpretation as a distal back-barrier lagoon, with the fining upward profile representing decreasing energy with gradual filling (e.g., [56]).

Differences in the clay mineralogy between the northern and southern samples can provide information about relative proximity to the paleoshore. Because kaolinite flocculates more readily in low salinities and montmorillonite flocculates more rapidly at high salinities [55,57], the difference in clay mineralogy can be related to the degree of fluvial input. The northern Pontotoc samples are kaolinite rich and the southern samples have a higher montmorillonite/kaolinite ratio, suggesting that the southern location was more proximal to the open ocean or experiencing relatively minor fluvial input, while the northern location was fed by a larger fluvial system or was more isolated from the open ocean.

5.1.2. Carbonaceous Sand Lithofacies

The clay matrix and carbonaceous material suggest a low energy location close to a terrestrial source. The upward decrease in clay content suggests an increase in energy over time. We interpret the Fe-cemented layers as diagenetic and non-diagnostic of depositional setting. The organic carbon content of this lithofacies and its position at the base of the measured section suggests that it represents the middle Ripley, which contains abundant lignitic sand and bedded lignite [21]. We interpret the paleoenvironment as a proximal back-barrier lagoon.

5.1.3. Wavy-Bedded Sand Lithofacies

Despite the abundance of sand, the alternating layers of more and less mud matrix indicate alternating energy during tidally influenced deposition. The cleaner sand represents higher energy during the dominant tide and the more mud-rich sand represents lower energy during the subordinate tide. Compared to typical instances of wavy and lenticular bedding, this lithofacies represents an overall relatively high-energy environment (e.g., [58]). The lack of pure mud and lack of subaerial exposure indicators suggests that deposition occurred in a shallow subtidal setting, likely a subtidal sand flat.

5.1.4. Massive Sand Lithofacies

The massive nature of this lithofacies is not particularly informative in terms of depositional environment, but lateral and vertical relationships with the sandy clay, wavy-bedded, and sandy packstone lithofacies, suggest a largely subtidal marine origin. Clay bedding and laminae potentially indicate isolated low energy periods. Rip-up clasts formed when a return to high-energy conditions eroded mud beds.

Where trace fossils are present, their diversity is low, supporting the relatively high-energy conditions indicated by the sedimentology [59]. Type 1 trace fossils (Figure 5E) likely represent two-dimensional expression of three-dimensional boxwork burrow systems. Even though the traces

are poorly preserved, the size, architecture, and wall with suggestions of pellets indicate that these are attributable to *Ophiomorpha* and are comparable to callianassid shrimp burrows within a shoreface environment [60–62]. Type 2 traces (Figure 5F) are most similar to concentrically laminated *Thalassinoides* described by Goldring [63]. *Thalassinoides* can be found in a range of marine settings, but is compatible with a shoreface environment [64].

5.1.5. Ripple-Laminated Sand Lithofacies

Ripple lamination indicates lower flow regime conditions in relatively shallow water. The lateral relationship to the wavy-bedded sand lithofacies suggests that the ripples represent a shoaling sand flat environment (e.g., [65]). Timing of slumping and microfaulting is difficult to determine because even recent seismicity would cause deformation along offsets due to the friable nature of the sand.

5.1.6. Sandy Packstone Lithofacies

The moderate energy depositional setting implied by packstone combined with an abundance of siliciclastic grains suggests an inner to middle shelf environment. The high diversity of fossils indicates normal marine conditions. The presence of *Sphenodiscus*, *Exogyra*, and *Hardouinia* indicate that this limestone belongs to the Chiwapa Member of the Ripley Formation [22].

Overall, the Ripley Fm in the field areas represents a barrier island to shelf system. This is similar to interpretations of the Ripley system to the east in Alabama [66].

5.2. Detrital Zircon Age Distributions and Provenance

The NS and SS contain Grenville-aged (~1200–980 Ma; [67]) detrital zircons at ~80.1% (Table 1; Figure 9). The next two largest age provinces represented in the data are the Acadian Orogeny (~450–320 Ma) at 6.9% and Mid-Continent Granite–Rhyolite (~1500–1350 Ma) at 6.8% (Table 1; Figure 9). Smaller peaks, in descending order, are the Gondwanan Terranes (~900–500 Ma) at 2.2%, Taconic (~490–440 Ma) at 1.5%, and all containing less than 1% per province are the Superior (> 2500 Ma), Trans-Hudson/Penokean (~1900–1800 Ma), Yavapai–Mazatzal (~1800–1600 Ma), and Alleghanian (~330–265 Ma) (Table 1; Figure 9).

North American zircon ages are well constrained according to the igneous province in which each grain originated (Figure 7). However, within the context of deep time, it is important to consider the possibility that sampled detrital zircons have been subjected to one or more cycles of weathering, transport, deposition, and lithification. Given that the youngest age from the Pontotoc zircons is Pennsylvanian, there is a possibility that most or all these grains have been recycled. It is also important to note that the four samples from northern Pontotoc were combined into a single population based on similar K–S results ($p > 0.05$) and the same approach was applied to the seven samples collected from the southern sampling locality (Figure 8). Despite the statistical similarity of the individual samples constituting the NS and the similarity of those constituting the SS, the K–S test comparing the NS and SS yielded a p -value of ~0.01. Likewise, MDS shows that the NS and SS are highly dissimilar to each other when compared to other published DZ data (Figure 10). This indicates that the NS and SS age spectra are different and possibly had slightly different sedimentary inputs. The main differences in the samples can be seen by comparing dominant age peaks in probability density plots (Figure 9). The most prominent DZ age peaks in the NS are a double peak at 1193 Ma and 1107 Ma, which is a characteristic age representing the Grenville (e.g., [52,68]). Age peaks of 447 Ma, representing Taconic ages (e.g., [69–71]), and 1426 Ma, representing Mid-Continent Granite–Rhyolite (e.g., [72,73]), are the second most significant peaks (Figure 9). In comparison, the two most dominant age peaks in the SS are at 1042 Ma and 337 Ma, which are Grenville and Acadian (e.g., [70,74]) in age (Figure 9). The next two most significant DZ age peaks in the SS are at 1182 Ma and 430 Ma, representing Grenville and Taconic ages, respectively (Figure 9).

There are four differences in the overall percentages of DZ ages between the NS and SS. The first is an 8.8% difference in Acadian (~450–320 Ma) sourced grains between the SS (1.8) and NS (10.6%);

Table 1; Figure 9). Next, the NS shows a larger percentage of Taconic (~490–440 Ma) aged grains at 3.3% compared to the 0.3% in the SS (Table 1; Figure 9). Third, the MCGRP ages (~1600–1350 Ma) are more prominent in the NS (9.9%) than in the SS (4.5%; Table 1; Figure 9). Finally, the SS shows no age spectra for the Yavapai–Mazatzal (~1800–1600 Ma) and Trans-Hudson/Penokean provinces (~1900–1800 Ma) compared to the NS (1.5% and 0.7% respectively; Table 1; Figure 9).

The Grenville double peaks (Figure 9) represent the orogenic events that bound a period of Adirondian magmatism (1180–1080 Ma) [75]. The first orogenic event is the Elzevierian Orogeny (1230–1180 Ma), followed by the back-arc tectonics of the Adirondian magmatic period and finally the continental–continental collision of the Grenville Orogeny (1080–980 Ma) [75]. Zircons eroded from Grenville basement rocks are prominent in the AFB (Figures 11 and 12; e.g., [1,48–50,76]).

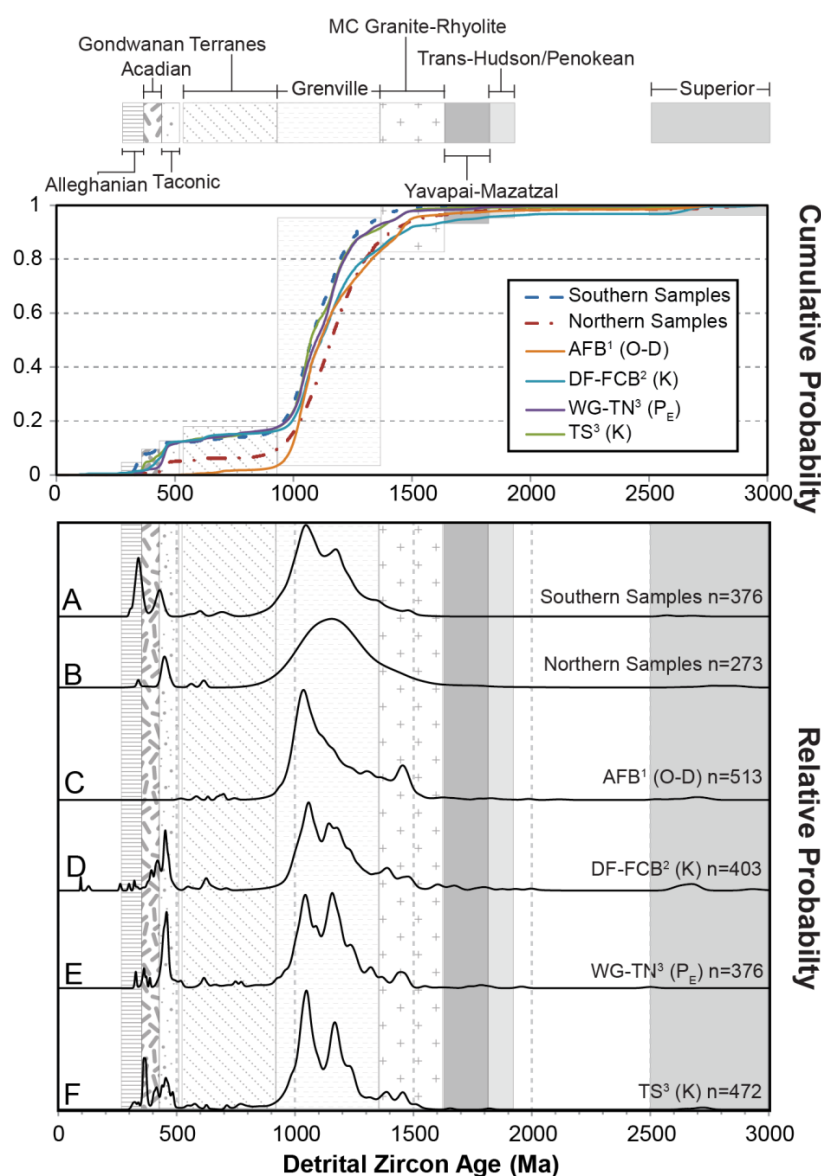


Figure 11. Stacked cumulative and normalized age-probability plots of detrital zircon from (A) SS, (B) NS, (C) Ordovician and Devonian strata in the Appalachian Foreland Basin (AFB);¹ [50]), (D) Cenomanian–Albian Dakota Fm from the FCB; ² [17]), (E) Paleocene Wilcox Group strata from Tennessee (WG–TN); ³ [1], (F) Cenomanian Tuscaloosa Sandstone (TS). Potential source regions are shown as vertical bars. Samples shown have K–S statistical *p*-values > 0.05 when compared to either the SS or NS.

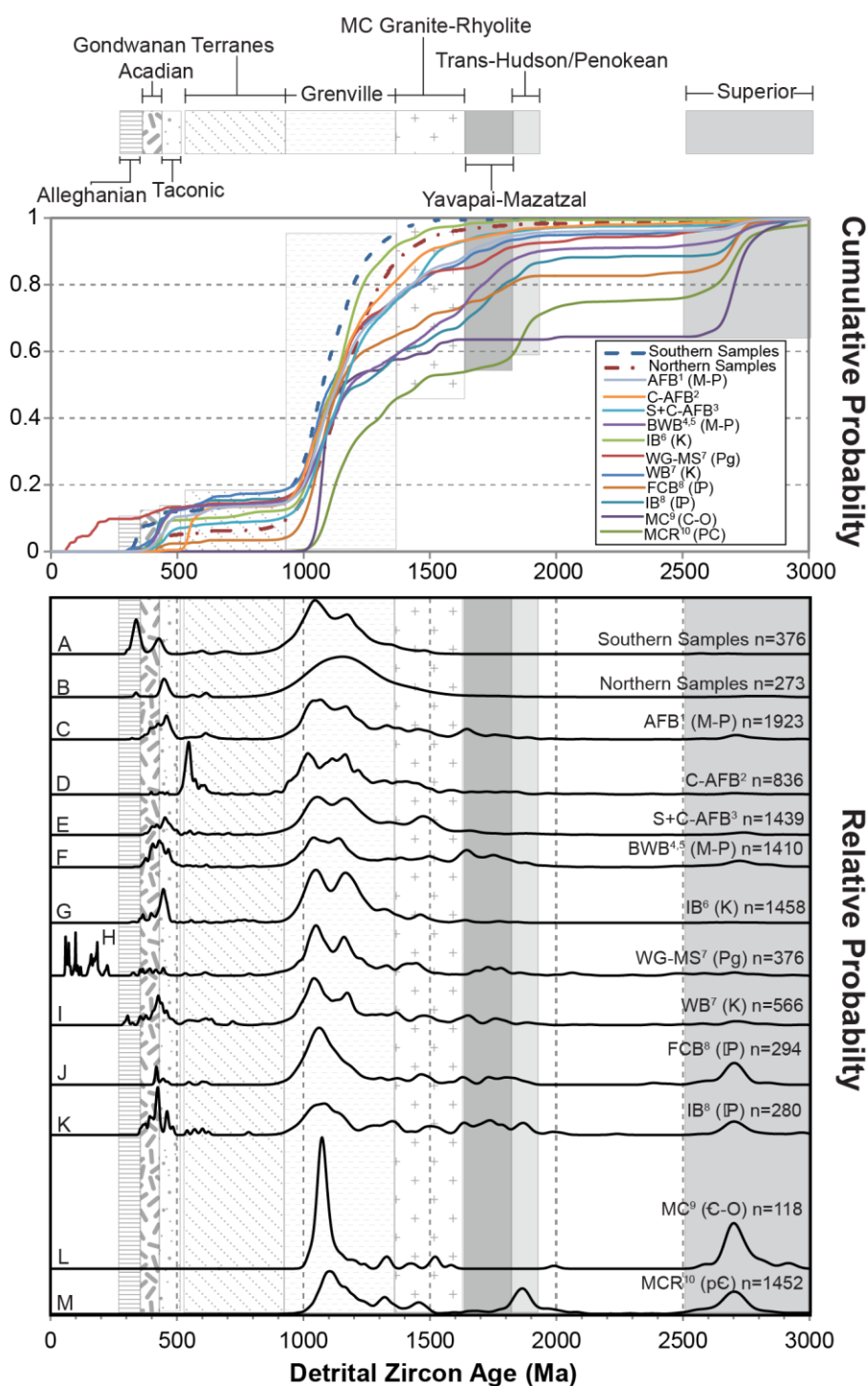


Figure 12. Stacked cumulative and normalized age-probability plots of detrital zircon from (A) SS, (B) NS, (C) Mississippian–Permian strata in the AFB; ¹ [50], (D) Paleozoic to Mesozoic strata in the central Appalachian Foreland Basin (C-AFB); ² [49], (E) Paleozoic to Mesozoic strata in the south and central Appalachian Foreland Basin (S+C-AFB); ³ [48], (F) Mississippian to Pennsylvanian strata from the Black Warrior Basin (BWB); ⁴ [46], ⁵ [47], (G) Cretaceous strata from the Illinois Basin (IB); ⁶ [3], (H) Paleocene Wilcox Group strata from Mississippi (WG-MS); ⁷ [1], (I) Cenomanian Woodbine Fm (WB), (J) Pennsylvanian Forest City Basin strata (FCB); ⁸ [45], (K) Pennsylvanian Illinois Basin (IB), (L) Cambrian to Ordovician Mid-Continent strata (MC); ⁹ [44], (M) Precambrian Mid-Continent Rift strata (MCR); ¹⁰ [43]. Potential source regions are shown as vertical bars. Samples shown have K–S statistical *p*-values < 0.05 when compared to either the NS or SS.

The SS contains 1.1% Alleghanian derived detrital grains (Table 1; Figure 9), which are comparable to the Cenomanian (100.5–93.9 Ma) Tuscaloosa Sandstone DZ age spectra, the Paleocene Wilcox Group from Tennessee DZ age spectra obtained by Blum and Pecha [1] (Figure 11E), and the Cenomanian–Albian (~113–100.5 Ma) Dakota Fm from Finzel [17] (Figure 11D). Alleghanian-aged grains within the SS suggest a sediment source from the Appalachian–Ouachita fold–thrust belt and drainage basin that routed sediment from the Appalachians to the northeastern MSE [1] and further west during the Late Cretaceous to deposit in the FCB (Figure 13) [17]. Alleghanian deformation extends from the southern Appalachians into New England and, before the continental-scale paleodrainage shift to the MSE, the Southern and New England Appalachians could have been sourcing the Albian and Cenomanian strata in the FCB dated by Finzel [17]. Then the paleodrainage shift deposited the Cretaceous and Paleocene strata of this study and Blum and Pecha [1]. Similarities with the Thomas et al. [50] detrital spectra (Figure 11C) indicate that the Upper Cretaceous and Paleogene strata in the MSE are likely sourced from the Ordovician and Devonian sandstones from the Taconic synorogenic clastic wedges of the southern Appalachians and show no source change during this time (Figure 11C).

A large Acadian age peak (~337 Ma; 10.6%) occurs in the SS along with a minor Taconic peak (~430 Ma; 0.3%). This is the opposite of the NS, which has a larger Taconic age peak (~447 Ma; 3.3%) and no Alleghanian-aged grains. Acadian-aged grains are present in the Pennsylvanian Illinois Basin deposits (Figure 12G,K; [3,45]), Albian and Cenomanian sandstone deposits in IA, AL, and MS (Figures 12H and 11D; [1,17]), and Paleocene paleo-river deposits from the GoM coastal plain (Figure 12H; [1]). Similar to the Taconic-aged grains, the Acadian-aged zircons may have been derived from recycling of Paleozoic strata from the AFB. It is interesting to note that the elongate kyanite grains found in the southern sample likely correlate with the detritus from the kyanite–staurolite amphibolite facies zones in the central–northern Appalachians, suggesting a more direct sediment source from the Appalachian Orogen or AFB [1,77]. Blum and Pecha [1] similarly noted a range in kyanite abundances in Cenomanian and Paleocene GoM samples.

The NS and SS show relatively minor input from Gondwanan Terranes (1.1% and 2.9%; i.e., Sabine and Suwanee blocks). Similarly, the Illinois Basin (Figure 12G,K; [3,45]), FCB (Figures 12J and 11D; [17,45]), and the Cenomanian and Paleocene MSE samples (Figures 12H and 11E; [1]) all contain very minor percentages of Gondwanan Terrane ages. When the Gondwanan Terranes accreted to southeastern Laurentia, foreland intracratonic and pericratonic basins accumulated sediment from the Appalachian–Ouachita Orogenic Belt and Gondwanan sources. Therefore, it is expected to see Gondwanan Terrane zircon ages within these basins [1,78,79].

All samples in Figures 11 and 12 show major to minor peaks in MCGRP ages (~1456–1354 Ma). The NS contains 9.9% MCGRP grains with an age peak of ~1426 Ma, while the SS contains 4.5% MCGRP grains and contains two lower age peaks of ~1354 Ma and ~1490 Ma. The appearance of a high percentage of MCGRP grains in the Ripley Formation suggests two possible sediment sources: (1) Paleozoic intracratonic basins or (2) the exposed Precambrian rocks within the MCGRP [73]. Paleozoic basin sediments that have undergone recycling before deposition, leading to a wide age spectrum (Archean to Cenozoic) of grains present in a single sample. The only outcrops of the MCGRP from which Mesoproterozoic grains may have originated are in the St. Francois Mountains (southeast Missouri), the highest points of the Arbuckle Mountains (south–central Oklahoma), and the Spavinaw Creek area (northeastern Oklahoma) [73]. Cenozoic subsidence and Quaternary southern tilting of the MSE resulted from the underlying Reelfoot Rift and would have created a direct sediment route from surrounding areas to the MSE. However, in the Late Cretaceous, MCGRP aged grains from Oklahoma and Missouri would have been following the western drainage patterns as described by Blum and Pecha [1] and Finzel [17], making recycled sediment from the intracratonic basins the most likely source of MCGRP aged zircons (Figure 13).

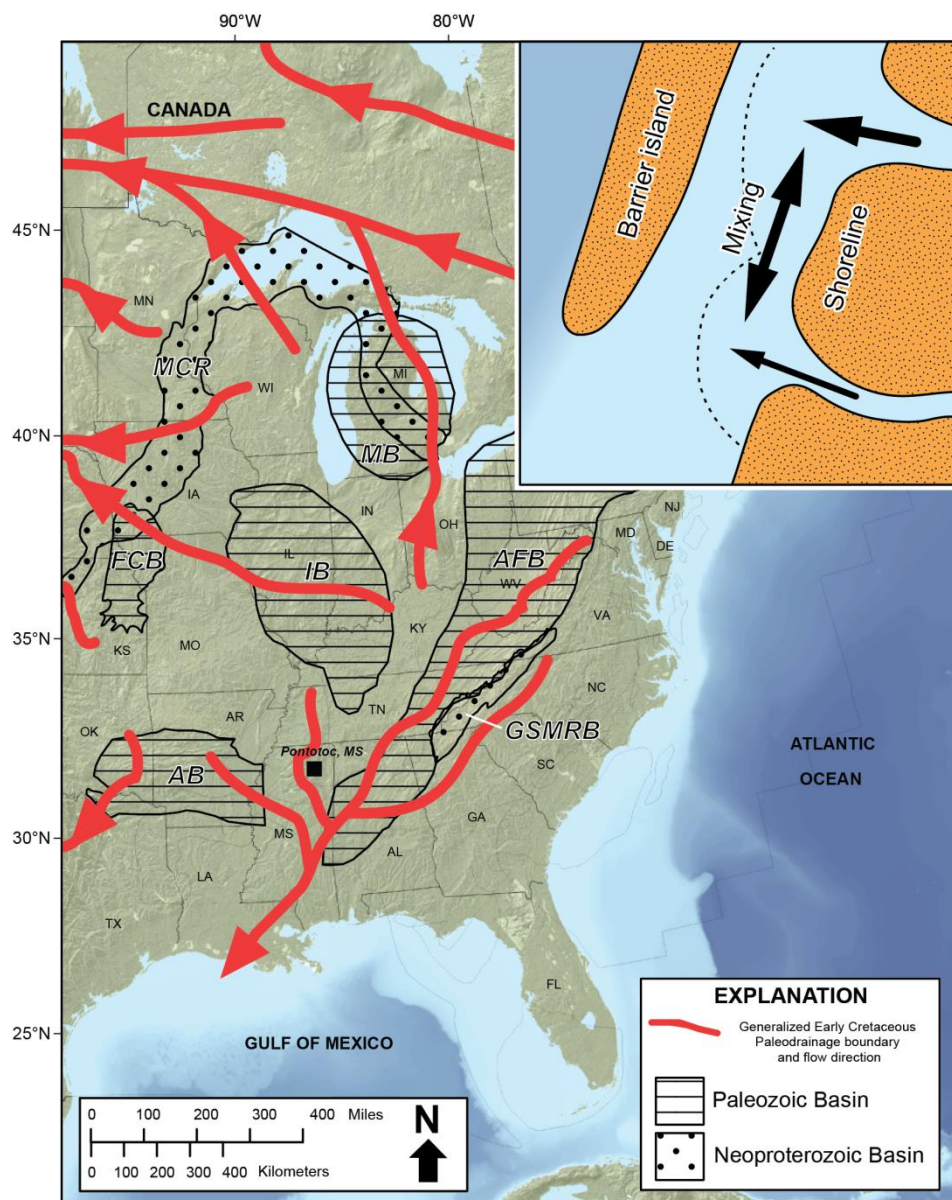


Figure 13. Map of the Paleozoic and Neoproterozoic basins of eastern North America. AB = Arkoma Basin, AFB = Appalachian Foreland Basin, FCB = Forest City Basin, GSMRB = Great Smokey Mountain Rift Basin, MB = Michigan Basin, MCR = Mid-Continent Rift. Modified from Coleman and Cahán [79]. Red lines indicate Late Cretaceous mid-continent paleodrainage and flow directions, modified from Blum and Pecha [1]. Inset: Generalized paleoenvironmental reconstruction of the region encompassing the northern and southern Pontotoc field sites (black square; see Figure 1B). Single-headed arrows represent fluvial input into back-barrier setting, thicknesses of the arrows represent relative volume of input based on salinity indicators from clay mineralogy. Dashed line represents approximate outline of subaqueous portion of deltas formed at river mouths. Double headed arrow represents mixing between the two fluvial sources.

Superior- and Wyoming-aged grains show prominent peaks in the northern Illinois Basin (Figure 12K; [45]), FCB (Figures 12J and 11D; [17,45]), and the Paleo-Tennessee Paleocene Wilcox Group samples (Figure 11E; [1]). A small population of Superior- and Wyoming-aged grains are observed in the Cenomanian Tuscaloosa sample of Blum and Pecha [1] (Figure 11F), the Paleocene Wilcox Tennessee and Mississippi paleo-River samples of Blum and Pecha [1] (Figure 11E), and the southern Illinois Maastrichtian McNairy Sandstone of Potter-McIntyre et al. [3] (Figure 12G). The lack

of Archean-aged grains in the Blum and Pecha [1] samples supports that Archean grains are recycled from lower Paleozoic strata [44]. Gleason et al. [80] suggested an Ordovician shift from Archean Superior Province and MCGRP ages to a dominant Appalachian–Grenville influx of sediment in western Oklahoma and central Arkansas. The Cenomanian Woodbine samples from Blum and Pecha [1] (Figure 12I) show a large input of recycled sediment from the Ouachita fold and thrust belt and could therefore explain the Superior signature in the Ripley Formation samples as a result of sediment input from the same region [1,80].

An influx of recycled sediment from the Ouachita fold and thrust belt is also supported by the work of Finzel [17] since Albian–Cenomanian Dakota Fm samples are geographically close to the Superior region. Finzel [17] collected Albian–Cenomanian Dakota Fm samples from eastern Nebraska and Western Iowa that are statistically similar to our NS. If Cenomanian samples that are closer to the Superior and MCGRP regions do not contain strong age ranges from those provinces as well, then Superior and MCGRP age signatures are the result of sediment recycling and not direct sediment sourcing (e.g., [1,17,80]). In addition, there is a complete absence of Yavapai–Mazatzal and Trans-Hudson/Penokean ages in the SS and only a small combined population in the NS (2.2% of the sample). The overall lack of Paleoproterozoic aged grains in the NS and SS, as well as a lack of these grains in the Pennsylvanian-aged strata described in Kissock et al. [45], indicates that there was likely no direct input into the north and northeastern MSE during the Maastrichtian from the south and southwestern North American igneous provinces where these grains originally crystallized (Figure 7). The small age peak in the NS (Figure 9) is attributed to recycling of Paleoproterozoic sediment into distal sources that then drained into the MSE.

The SS is statistically indistinguishable from the Cenomanian Tuscaloosa Formation DZ ages according to K–S results ($p = 0.718$) and the two samples are nearest neighbors according to MDS results (Figure 10). The SS is also statistically the same as the Paleo-Tennessee Paleocene Wilcox Group samples DZ ages [1] according to K–S results ($p = 0.165$) and are second nearest neighbors according to MDS results (Figure 10). This statistical compatibility supports the Blum and Pecha [1] east-to-west drainage system extending from the Appalachian Mountains into the Western Interior Seaway (WIS) from the Permian through the Early Cretaceous. At the end of the Early Cretaceous, the retreat of the WIS rerouted all drainage from west to east and the southern river systems joined the ancestral Mississippi River and other Appalachian-sourced systems [1].

Similar to the SS, an Appalachian source for the NS is suggested by its minimum dissimilarities to the Southern and Central Appalachians and Mississippian–Permian strata of the AFB (Figure 10). In this case, MDS results do not entirely agree with K–S results, which indicate that the NS is indistinguishable from Albian–Cenomanian strata of the Dakota Fm in western Iowa and eastern Nebraska ($p = 0.083$) and Ordovician–Devonian strata of the AFB ($p = 0.052$). This is not problematic, however, because all results support an Appalachian–Ouachita cordillera source that deposited sediment in the FCB in the Albian and Cenomanian, and shifted to MSE deposition in the Maastrichtian due to paleodrainage reconfiguration (Figure 13) [1,17]. Since the NS and SS are similar to the detrital age spectra of Blum and Pecha [1], Finzel [17], and Thomas et al. [50], i.e., sourced from the Appalachian–Ouachita foreland basin, Ripley Fm sediments are likely sourced from the same areas (Figures 11 and 13).

The difference between NS and SS K–S and MDS results at first seems to argue against a correlation between the northern and southern sites. However, recall that many of the individual northern and southern samples are statistically indistinguishable from each other. Given the back-barrier depositional setting, we attribute differences in DZ age spectra to influence from different fluvial inputs into the same lagoonal system, while similarities between DZ age spectra resulted from shared source regions and sediment mixing. In this scenario, we interpret a southern fluvial system dominantly draining more easterly locations (mostly the AFB), and a northern fluvial system that drained a more westerly area, including the AFB, but with greater input from Mid-Continent, Trans-Hudson, Penokean, and Yavapai–Mazatzal provinces (Figure 13—inset). This also agrees with the lower salinity northern

site representing a greater volume of fluvial input because of the correlation between drainage basin area and discharge [81].

6. Conclusions

Lithofacies analysis of the Cretaceous Ripley Formation in Pontotoc County, MS indicates a barrier island to shelf system with volcanoclastic deposits preserved in a back-barrier environment. While relatively pure bentonites were mined from below the Chiwapa Sandstone Member of the Ripley Formation in Pontotoc County in the 1940s, two newly discovered sandy expansive clay deposits are located above the CSM, but are likely not minable. These new deposits, nevertheless, are important because they record evidence of some of the youngest known Late Cretaceous volcanism in the Mississippi Embayment. While our samples did not yield volcanic zircons, we were able to perform a DZ study of a northern sample population (NS) and southern sample population (SS) to determine provenance of the Ripley Formation. DZ age spectra ranged from 2870 Ma (Mesoarchean) to 305 Ma (Late Pennsylvanian) in age with primary concentrations from the Grenville (80%), and Acadian Orogeny (7%). The NS yielded higher amounts of Taconic (3.3%) and Mid-Continent Granite–Rhyolite province (9.9%) compared to the SS (0.3% and 4.5% respectively). The SS yielded significantly higher amounts of Acadian-aged grains (10.6%) relative to the NS (1.8%). This spectrum of ages with very limited amounts of Superior, Trans-Hudson/Penokean, and Yavapai–Mazatzal leads to the conclusion that the sediment input into the northeastern MSE during the late Maastrichtian was likely sourced from the AFB with minor input from the mid-continent region by routing sediment through the Reelfoot Rift trough at the apex of the ancestral Mississippi River. AFB sourcing is based on the statistical similarities to the DZ ages of Albian–Paleocene strata of the MSE and FCB and the upper Maastrichtian strata of Pontotoc County, MS, which had not previously been analyzed in northeastern Mississippi. The similar DZ ages of this study compared to Albian–Cenomanian strata of the FCB support an east-to-west drainage system that transported sediment across the continent before the early Paleogene.

The high abundance of heavy minerals, such as muscovite and kyanite, along with the large number of Acadian- and Alleghanian-aged grains within the sample also support that sediment sources during deposition of upper Ripley strata included the AFB.

Supplementary Materials: The following are available online at <http://www.mdpi.com/2076-3263/10/2/80/s1>, Table S1: Analytical results (isotopic ratios) and calculated U–Pb ages for DZ from samples of this study. Samples analyzed at Washington State University (WSU) following the procedures described in Chang et al. [82] and samples analyzed at the University of Arizona (UA) following the procedures described in Gehrels et al. [83] and Gehrels et al. [84]. Reduced isotopic ratios are corrected for drift and fractionation effects. Errors reported are corrected based on analytical error and on observed variation of analyzed standards. Table S2: K–S statistics, (a) comparing each of the 11 individual northern and southern samples to all of the others; (b) comparing the combined NS and SS values; (c) comparing the NS and SS analyses to published data sets, citations available in the manuscript.

Author Contributions: Conceptualization, J.N.G.; methodology, J.N.G.; formal analysis, E.J.V.; funding acquisition, E.J.V. and J.N.G.; investigation, E.J.V., J.N.G., B.F.P.; project administration, J.N.G.; supervision, J.N.G.; visualization, E.J.V., J.N.G., B.F.P.; writing—original draft preparation, E.J.V.; writing—review and editing, J.N.G., B.F.P., D.H.M., I.H.W. All authors have read and agreed to the published version of the manuscript.

Funding: This research was funded by the University of Mississippi Department of Geology and Geological Engineering, the Geological Society of America Graduate Student Research Grants, and the Gulf Coast Association of Geological Societies Student Grants.

Acknowledgments: This paper is the product of a Master’s thesis by E.J.V. at the University of Mississippi. We thank Charles Swann and the MMRI, Chayan Lahiri, and Poe Brothers Trucking, Inc. for assistance in the field as well as access to the sample locations. We would like to thank the Gulf Coast Association of Geological Societies for funding part of this research. We also thank Barry Shaulis from the University of Arkansas Trace Element and Radiogenic Isotope Lab, George Kamenov at the University of Florida Geochronology Laboratory, and Paul O’Sullivan from GeoSep Services for their help acquiring U–Pb analyses. We also thank two anonymous reviewers for their helpful comments that greatly improved the manuscript.

Conflicts of Interest: The authors declare no conflict of interest. The funders had no role in the design of the study; in the collection, analyses, or interpretation of data; in the writing of the manuscript, or in the decision to publish the results.

Appendix A North American Provenance Terranes

Detrital Zircon (DZ) provenance studies are possible because DZ ages correspond to crystallization ages of the individual cratonic elements that amalgamated over billions of years to form the continents in their current configurations [52]. Several igneous provinces are recognized in North America (Figure 7). The following are descriptions of these igneous provinces referred to in this manuscript with citations.

Appendix A.1 Superior (> 2500 Ma)

The Superior Province in North America (Figure 7) is the result of multiple episodes of subduction that led to the amalgamation of the world's largest Archean craton (e.g., [85–89]). East–west trending belts of extensive and alternating metasedimentary and granite-greenstones along with high-grade plutonic terranes compose the Superior Province [72,85,90,91]. Geochemical evidence shows that the Superior Province decreases in age to the south [91].

Appendix A.2 Trans-Hudson/Penokean (~1900–1800 Ma)

The Penokean Orogeny (Figure 7) occurred between 1880–1820 Ma and outcrops in central Minnesota and Northern Wisconsin [92–95]. The Trans-Hudson Orogeny is a well-preserved Mesoproterozoic orogenic belt that stretches from central–northern United States and into Canada [93]. Trans-Hudson aged rocks outcrop extensively in Saskatchewan in Southern Canada (Figure 7; [96]).

Appendix A.3 Yavapai–Mazatzal (~1800–1600 Ma)

The late Paleoproterozoic was a time of large-scale crustal growth in North America. During this time, three provinces (Mojave, Yavapai, and Mazatzal; Figure 7) were accreted to the Wyoming Craton along its southern boundary (e.g., [52,97–99]). Detrital zircon grains that fall within this age range are likely recycled from Pennsylvanian basins, which had also been recycled from Neoproterozoic and early Proterozoic quartzites (e.g., [3,43]).

Appendix A.4 Mid-Continent Granite–Rhyolite (~1500–1350 Ma)

The Mid-Continent Granite–Rhyolite Province (MCGRP) is a Precambrian basement terrane beneath southwestern Ontario extending south to Arkansas, east to Ohio, and west to Kansas, Oklahoma, and the Texas panhandle (Figure 7; [73]). The MCGRP in the east contains high-silica rhyolite to dacite with granite having U–Pb ages of ~1470 Ma. The southern MCGRP has the same composition; however U–Pb ages are ~1390–1340 Ma westward and only show major episodes of magmatism in the south-central mid-continent region [72,73,100]. These Precambrian basement rocks show no deformation or metamorphism [73].

Appendix A.5 Grenville (~1200–980 Ma)

The Grenville province extends from northern Quebec to northern Mexico (Figure 7; Rivers, 1997). The Grenville Orogeny formed during late Mesoproterozoic convergence along the margin of Laurentia during the assembly of Rodinia [52]. The Appalachian Mesoproterozoic basement rocks that compose the southeastern United States differ from Canadian Grenvillian rocks because the Appalachian massifs experienced Paleozoic metamorphism and deformation due to orogenesis [67,68]. Grenville-age grains are common in Paleozoic sedimentary basins because of the recycling of the grains caused by the Paleozoic Taconic, Acadian, and Alleghanian orogenies and redeposition in different basins and the overall large amount of zircons contained by Grenvillian rocks (e.g., [3,45,46,48,101]).

Appendix A.6 Gondwanan Terranes (~900–540 Ma)

There are no Laurentian source terranes that are Neoproterozoic in age; however, there are Gondwanan Terranes, such as the Carolina (Figure 7; southern Appalachians; e.g., [102]), Suwanee

(Figure 7; Florida; e.g., [103–105]), and Sabine (Figure 7; Texas–Louisiana; e.g., [106]). Neoproterozoic terrane accretion is the result of the collision of Laurentia and Gondwana [102,106]. The Carolina terrane is a volcanic island arc along the southern Appalachian orogen that consists of basalts and basaltic andesites intruded by mafic–ultramafic plutonic complexes [102]. In the northern Suwanee terrane, Paleozoic sedimentary packages are Gondwanan-derived based on lithostratigraphy [103–105], fossil assemblages [107,108], paleomagnetic data [109], and detrital zircon data [110]. The Sabine terrane is a continental crustal block underlying the Gulf Coastal Plain (GCP) and within the Ouachita orogenic belt [106]. The composition of the Sabine terrane is poorly constrained because it lies under ~3.5 km of sedimentary cover [111]. However, Clift et al. [111] suggest that the Sabine terrane is not an exotic terrane, but is an extension of the Mazatzal due to rifting.

Appendix A.7 Taconic (~490–440 Ma)

Igneous activity related to the Taconic Orogeny occurred from the late Cambrian to the early Silurian (e.g., [69,70,112]). Taconic igneous rocks are characteristically different in the northern, central, and southern Appalachians (Figure 7). Two distinct groups of igneous rocks make up the northern Appalachians: (1) mafic and ultramafic rocks to the west, and (2) gneissic domes that overlay other volcanic and plutonic rocks (e.g., [113–116]). Igneous rocks of the southern Appalachians include multiple granitic plutonic intrusions and two suites of Blue Ridge gneisses and schists: a tonalitic and dioritic suite and mafic-ultramafic suite [69]. Deformation in the southern Appalachians is hard to discern due to later Alleghanian activity and the small amount of well-preserved Ordovician rocks, but is more prominent within the Blue Ridge and Piedmont than the AFB [69].

Appendix A.8 Acadian (~420–350 Ma)

The Acadian Orogeny spans from the late Silurian to early Carboniferous [70,74] and characteristically includes flysch and molasse deposits, episodic volcanism, folding and faulting, pulses of plutonism, and several periods of metamorphism [77]. Volcanic rocks of the Acadian Orogeny primarily outcrop in New England in two belts: the Piscataquia volcanic belt (e.g., [117–119]) and the coastal volcanic belt (e.g., [120–122]). Acadian volcanics also appear in the Talladega belt in Alabama in the southern Appalachians (Figure 7; [77]).

Appendix A.9 Alleghanian (~330–265 Ma)

The Alleghanian Orogeny occurred from the Late Mississippian to Permian when Africa collided with North America and resulted in the progression of the southern and central Appalachians cratonward as a single crystalline thrust sheet, resulting in foreland basin deformation [123]. The Alleghanian Orogeny is differentiated based on western and eastern characteristics. The western belt includes folds and thrust faults that continue into North American cratonic sedimentary rocks in the southern and central Appalachians (Figure 7; [124]). To the east, pre-Alleghanian metamorphic rocks make up a complex allochthonous belt [48,124]. Historic succession of the Alleghanian Orogeny is recorded in the synorogenic clastic wedges that comprise the AFB [125].

References

1. Blum, M.; Pecha, M. Mid-cretaceous to paleocene North American drainage reorganization from detrital zircons. *Geology* **2014**, *42*, 607–610. [[CrossRef](#)]
2. Blum, M.D.; Milliken, K.T.; Pecha, M.A.; Snedden, J.W.; Frederick, B.C.; Galloway, W.E. Detrital-zircon records of Cenomanian, Paleocene, and Oligocene Gulf of Mexico drainage integration and sediment routing: Implications for scales of basin-floor fans. *Geosphere* **2017**, *13*, 2169–2205. [[CrossRef](#)]
3. Potter-McIntyre, S.L.; Breeden, J.R.; Malone, D.H. A Maastrichtian birth of the Ancestral Mississippi River system: Evidence from the U-Pb detrital zircon geochronology of the McNairy Sandstone, Illinois, USA. *Cretac. Res.* **2018**, *91*, 71–79. [[CrossRef](#)]

4. Cushing, E.M.; Boswell, E.H.; Hosman, R.L. General geology of the Mississippi embayment. *U. S. Geol. Surv. Prof. Pap.* **1964**, *448-B*, 448.
5. Dockery, D.T.; Thompson, D.E. *The Geology of Mississippi*; University of Mississippi Press: Oxford, MS, USA, 2017.
6. Swann, C.T.; Mississippi Mineral Resources Institute, University, MS, USA. Personal communication, 2017.
7. Reed, J.C.; Wheeler, J.O.; Tucholke, B.E. *Decade of North American Geology Geologic Map of North America—Perspectives and Explanation*; The Geological Society of America: Boulder, CO, USA, 2005; pp. 1–28.
8. Ervin, C.P.; McGinnis, L.D. Reelfoot rift: Reactivated precursor to the Mississippi embayment. *Bull. Geol. Soc. Am.* **1975**, *86*, 1287–1295. [[CrossRef](#)]
9. Cox, R.T. Evidence of late Cenozoic activity along the Bolivar-Mansfield tectonic zone, midcontinent, USA. *Compass* **1988**, *65*, 207–214.
10. Csontos, R.; Van Arsdale, R.; Cox, R.; Waldron, B. Reelfoot rift and its impact on Quaternary deformation in the central Mississippi River valley. *Geosphere* **2008**, *4*, 145–158. [[CrossRef](#)]
11. Cox, R.T.; Van Arsdale, R.B.; Harris, J.B.; Larsen, D. Neotectonics of the southeastern Reelfoot rift zone margin, central United States, and implications for regional strain accommodation. *Geology* **2001**, *29*, 419–422. [[CrossRef](#)]
12. Chiu, S.C.C.; Chiu, J.M.; Johnston, A.C. Seismicity of the southeastern margin of Reelfoot rift, central United States. *Seismol. Res. Lett.* **1997**, *68*, 785–794. [[CrossRef](#)]
13. Dart, R.L.; Swolfs, H.S. Contour mapping of relic structures in the Precambrian basement of the Reelfoot rift, North American midcontinent. *Tectonics* **1998**, *17*, 235–249. [[CrossRef](#)]
14. Howe, J.R.; Thompson, T.L. Tectonics, sedimentation, and hydrocarbon potential of the Reelfoot Rift. *Oil Gas J.* **1984**, *82*, 179–190.
15. Howe, J.R. Tectonics, Sedimentation, and Hydrocarbon Potential of the Reelfoot Aulacogen. Master's Thesis, University of Oklahoma, Norman, OK, USA, 1985.
16. Cox, R.T.; Van Arsdale, R.B. The Mississippi Embayment, North America: a first order continental structure generated by the Cretaceous superplume mantle event. *J. Geodyn.* **2002**, *34*, 163–176. [[CrossRef](#)]
17. Finzel, E.S. Detrital zircons from Cretaceous midcontinent strata reveal an Appalachian Mountains-Cordilleran foreland basin connection. *Lithosphere* **2014**, *6*, 378–382. [[CrossRef](#)]
18. Cox, R.T.; Van Arsdale, R.B. Hotspot origin of the Mississippi embayment and its possible impact on contemporary seismicity. *Eng. Geol.* **1997**, *46*, 201–216. [[CrossRef](#)]
19. Malone, D.H.; Craddock, J.P.; Howell, B.A. Detrital zircon U/Pb provenance of the Lower Cretaceous Cloverly Formation, Big Horn and Powder River Basins, Wyoming. *Geol. Soc. Am. Abstr. Programs* **2013**, *45*, 584.
20. Sloss, L.L. Forty years of sequence stratigraphy. *Spec. Pap. Geol. Soc. Am.* **1988**, *253*, 51–55. [[CrossRef](#)]
21. Priddy, R.R. Pontotoc County Mineral Resources. *Mississippi State Geol. Surv. Bull.* **1943**, *54*, 139.
22. Mellen, F.F. Cretaceous Shelf Sediments of Mississippi. *Mississippi State Geol. Surv. Bull.* **1958**, 112.
23. Swann, C.T.; Dew, J.J. Geology of the Troy, Miss. 7.5 Minute Topographic Quadrangle Chickasaw and Pontotoc Counties Mississippi. *Mississippi Miner. Resour. Inst. Open File Rep.* **09-2S** **2009**, 4–11.
24. Walker, J.D.; Geissman, J.W.; Bowring, S.A.; Babcock, L.E. Geologic Time Scale v. 5.0. 2018.
25. Dockery, D.T. Mesozoic stratigraphic units in Mississippi. *Mississippi Geol.* **2008**, *17*, 1–8.
26. Paces, J.B.; Miller, J.D. Precise U-Pb ages of Duluth Complex and related mafic intrusions, northeastern Minnesota: geochronological insights to physical, petrogenetic, paleomagnetic, and tectonomagmatic processes associated with the 1.1 Ga Midcontinent Rift system. *J. Geophys. Res.* **1993**, *98*. [[CrossRef](#)]
27. Black, L.P.; Kamo, S.L.; Williams, I.S.; Mundil, R.; Davis, D.W.; Korsch, R.J.; Foudoulis, C. The application of SHRIMP to Phanerozoic geochronology; a critical appraisal of four zircon standards. *Chem. Geol.* **2003**, *200*, 171–188. [[CrossRef](#)]
28. Shaulis, B.; Lapen, T.J.; Toms, A. Signal linearity of an extended range pulse counting detector: Applications to accurate and precise U-Pb dating of zircon by laser ablation quadrupole ICP-MS. *Geochem. Geophys. Geosyst.* **2010**, *11*, 1–12. [[CrossRef](#)]
29. Sláma, J.; Košler, J.; Condon, D.J.; Crowley, J.L.; Gerdes, A.; Hanchar, J.M.; Horstwood, M.S.A.; Morris, G.A.; Nasdala, L.; Norberg, N.; et al. Plešovice zircon—A new natural reference material for U-Pb and Hf isotopic microanalysis. *Chem. Geol.* **2008**, *249*, 1–35. [[CrossRef](#)]
30. Ludwig, K.R. Isoplot 3.75 2012. Available online: http://www.bgc.org/isoplot_etc/isoplot.html (accessed on 17 January 2020).

31. Gehrels, G.; Way, I. Cumulative Age Probability Plots. Available online: <https://drive.google.com/file/d/0B9ezu34P5h8eQk04SWEwYTA2eWM/view> (accessed on 17 January 2020).
32. Gehrels, G. K-S Test. Available online: <https://drive.google.com/file/d/0B9ezu34P5h8eLWpNYldGMWp3dEU/view> (accessed on 17 January 2020).
33. Guynn, J.; Gehrels, G. Comparison of Detrital Zircon Age Distributions Using the K-S Test. Available online: https://docs.google.com/document/d/1MYwm8GcdYFOsfNV62B6PULb_-g2r1AS3vmm4gHMOFxfg/preview (accessed on 17 January 2020).
34. Vermeesch, P. Dissimilarity measures in detrital geochronology. *Earth Sci. Rev.* **2018**, *178*, 310–321. [[CrossRef](#)]
35. Sircombe, K.N.; Hazelton, M.L. Comparison of detrital zircon age distributions by kernel functional estimation. *Sediment. Geol.* **2004**, *171*, 91–111. [[CrossRef](#)]
36. Vermeesch, P. Multi-sample comparison of detrital age distributions. *Chem. Geol.* **2013**, *341*, 140–146. [[CrossRef](#)]
37. Vermeesch, P.; Resentini, A.; Garzanti, E. An R package for statistical provenance analysis. *Sediment. Geol.* **2016**, *336*, 14–25. [[CrossRef](#)]
38. Spencer, C.J.; Kirkland, C.L. Visualizing the sedimentary response through the orogenic cycle: A multidimensional scaling approach. *Lithosphere* **2016**, *8*, 29–37. [[CrossRef](#)]
39. Vermeesch, P.; Garzanti, E. Making geological sense of “Big Data” in sedimentary provenance analysis. *Chem. Geol.* **2015**, *409*, 20–27. [[CrossRef](#)]
40. Arboit, F.; Collins, A.S.; Morley, C.K.; King, R.; Amrouch, K. Detrital zircon analysis of the southwest Indochina terrane, central Thailand: Unravelling the Indosinian orogeny. *Bull. Geol. Soc. Am.* **2016**, *128*, 1024–1043. [[CrossRef](#)]
41. Saylor, J.E.; Jordan, J.C.; Sundell, K.E.; Wang, X.; Wang, S.; Deng, T. Topographic growth of the Jishi Shan and its impact on basin and hydrology evolution, NE Tibetan Plateau. *Basin Res.* **2018**, *30*, 544–563. [[CrossRef](#)]
42. Xu, J.; Snedden, J.W.; Stockli, D.F.; Fulthorpe, C.S.; Galloway, W.E. Early miocene continental-scale sediment supply to the gulf of Mexico basin based on detrital zircon analysis. *Bull. Geol. Soc. Am.* **2017**, *129*, 3–22. [[CrossRef](#)]
43. Craddock, J.P.; Konstantinou, A.; Vervoort, J.D.; Wirth, K.R.; Davidson, C.; Finley-Blasi, L.; Juda, N.A.; Walker, E. Detrital zircon provenance of the Mesoproterozoic Midcontinent Rift, Lake Superior region, USA. *J. Geol.* **2013**, *121*, 57–73. [[CrossRef](#)]
44. Konstantinou, A.; Wirth, K.R.; Vervoort, J.D.; Malone, D.H.; Davidson, C.; Craddock, J.P. Provenance of quartz arenites of the early Paleozoic midcontinent region, USA. *J. Geol.* **2014**, *122*, 201–216. [[CrossRef](#)]
45. Kissock, J.K.; Finzel, E.S.; Malone, D.H.; Craddock, J.P. Lower-Middle Pennsylvanian strata in the North American midcontinent record the interplay between erosional unroofing of the Appalachians and eustatic sea-level rise. *Geosphere* **2018**, *14*, 141–161. [[CrossRef](#)]
46. Xie, X.; O’Connor, P.M.; Alsleben, H. Carboniferous sediment dispersal in the Appalachian–Ouachita juncture: Provenance of selected late Mississippian sandstones in the Black Warrior Basin, Mississippi, United States. *Sediment. Geol.* **2016**, *342*, 191–201. [[CrossRef](#)]
47. Gifford, J.N.; Platt, B.F.; Yarbrough, L.; O’Reilly, A.; Al Harthy, M.H.M. Integrating petrography, x-ray fluorescence, and U-Pb detrital zircon geochronology to interpret provenance of the Mississippian Hartselle Sandstone, USA. *J. Geol.* (under review).
48. Park, H.; Barbeau, D.L.; Rickenbaker, A.; Bachmann-Krug, D.; Gehrels, G. Application of foreland basin detrital-zircon geochronology to the reconstruction of the southern and central Appalachian orogen. *J. Geol.* **2010**, *118*, 23–44. [[CrossRef](#)]
49. Eriksson, K.A.; Campbell, I.H.; Palin, J.M.; Allen, C.M.; Bock, B. Evidence for multiple recycling in Neoproterozoic through Pennsylvanian sedimentary rocks of the central Appalachian basin. *J. Geol.* **2004**, *112*, 261–276. [[CrossRef](#)]
50. Thomas, W.A.; Gehrels, G.E.; Greb, S.F.; Nadon, G.C.; Satkoski, A.M.; Romero, M.C. Detrital zircons and sediment dispersal in the Appalachian foreland. *Geosphere* **2017**, *13*, 2206–2230. [[CrossRef](#)]
51. Huff, W.D. K-bentonites: A review. *Am. Mineral.* **2016**, *101*, 43–70. [[CrossRef](#)]
52. Whitmeyer, S.J.; Karlstrom, K.E. Tectonic model for the Proterozoic growth of North America. *Geosphere* **2007**, *3*, 220–259. [[CrossRef](#)]

53. Dickinson, W.R.; Gehrels, G.E. U-Pb ages of detrital zircons in Jurassic eolian and associated sandstones of the Colorado Plateau: Evidence for transcontinental dispersal and intraregional recycling of sediment. *Geol. Soc. Am. Bull.* **2009**, *121*, 408–433. [[CrossRef](#)]
54. Alsalem, O.B.; Fan, M.; Zamora, J.; Xie, X.; Griffin, W.R. Erratum: Paleozoic sediment dispersal before and during the collision between Laurentia and Gondwana in the Fort Worth Basin, USA. *Geosphere* **2018**, *14*, 1988–1989. [[CrossRef](#)]
55. Pryor, W.; Vanwie, W.A. The “Sawdust Sand”; an Eocene sediment of floccule origin. *J. Sediment. Res.* **1971**, *41*, 763–769. [[CrossRef](#)]
56. Finkelstein, K.; Ferland, M.A. Back-barrier response to sea-level rise, eastern shore of Virginia. In *Sea-Level Fluctuation and Coastal Evolution, SEPM Special Publication 41*; Nummendal, D., Pilkey, O.H., Howard, J.D., Eds.; SEPM: Tulsa, Ok, USA, 1987; pp. 145–155.
57. Hahn, H.H.; Stumm, W. The role of coagulation in natural waters. *Am. J. Sci.* **1970**, *268*, 354–368. [[CrossRef](#)]
58. Howard, J.D.; Reineck, H.E. Depositional facies of high-energy beach-to-offshore sequence: Comparison with low-energy sequence. *Am. Assoc. Pet. Geol. Bull.* **1981**, *65*, 807–830. [[CrossRef](#)]
59. Buatois, L.A.; Mángano, M.G. *Ichnology: Organism-Substrate Interactions in Space and Time*; Cambridge University Press: Cambridge, UK, 2011; ISBN 9780521855556.
60. Frey, R.W.; Howard, J.D.; Pryor, W.A. Ophiomorpha: its morphologic, taxonomic, and environmental significance. *Palaeogeogr. Palaeoclimatol. Palaeoecol.* **1978**, *23*, 199–229. [[CrossRef](#)]
61. Pollard, J.E.; Goldring, R.; Buck, S.G. Ichnofabrics containing Ophiomorpha: significance in shallow-water facies interpretation. *J. Geol. Soc. London.* **1993**, *150*, 149–164. [[CrossRef](#)]
62. Bromley, R.G.; Ekdale, A.A. Ophiomorpha irregulaire (trace fossil): Redescription from the Cretaceous of the Book Cliffs and Wasatch Plateau, Utah. *J. Paleontol.* **1998**, *72*, 773–778. [[CrossRef](#)]
63. Goldring, R. The sedimentological significance of concentrically laminated burrows from Lower Cretaceous Ca-bentonites, Oxfordshire. *J. Geol. Soc. Lond.* **1996**, *153*, 255–263. [[CrossRef](#)]
64. Pemberton, S.G.; MacEachern, J.A.; Dashtgard, S.E.; Bann, K.L.; Gingras, M.K.; Zonneveld, J.P. Shorefaces. In *Trace Fossils as Indicators of Sedimentary Environments*; Knaust, D., Bromley, R.G., Eds.; Elsevier: Amsterdam, The Netherlands, 2012; pp. 563–603.
65. Evans, G. Intertidal Flat Deposits of the Wash, Western Margin of the North Sea. In *Tidal Deposits*; Ginsburg, R.N., Ed.; Springer: Berlin/Heidelberg, Germany, 1975; pp. 13–20.
66. Skotnicki, M.C.; King, D.T. Depositional facies and eustatic effects in Upper Cretaceous (Maastrichtian) Ripley Formation, central and eastern Alabama. *Trans. Gulf Coast Assoc. Geol. Soc.* **1989**, *39*. [[CrossRef](#)]
67. Rivers, T. Lithotectonic elements of the Grenville Province: Review and tectonic implications. *Precambrian Res.* **1997**, *86*, 117–154. [[CrossRef](#)]
68. Tollo, R.P.; Corriveau, L.; McLelland, J.; Bartholomew, M.J. Proterozoic tectonic evolution of the Grenville orogeny in North America: an introduction. In *Proterozoic Tectonic Evolution of the Grenville Orogen in North America, GSA Memoir 197*; Tollo, R.P., McLelland, J., Corriveau, L., Bartholomew, M.J., Eds.; Geological Society of America: Boulder, CO, USA, 2004; pp. 1–18.
69. Drake, A.A.; Sinha, A.K.; Laird, J.; Guy, R.E. The Taconic orogen. In *The Appalachian–Ouachita Orogen in the United States*; Hatcher, R.D., Thomas, W.A., Viele, G.W., Eds.; Geological Society of America: Boulder, CO, USA, 1989; pp. 101–177.
70. Miller, C.F.; Hatcher, R.D.; Ayers, J.C.; Coath, C.D.; Harrison, T.M. Age and zircon inheritance of eastern blue ridge plutons, southwestern North Carolina and northeastern Georgia, with implications for magma history and evolution of the southern appalachian orogen. *Am. J. Sci.* **2000**, *300*, 142–172. [[CrossRef](#)]
71. Sinha, A.K.; Hanan, B.B.; Wayne, D.M. Igneous and metamorphic U-Pb zircon ages from the Baltimore mafic complex, Maryland Piedmont. In *The Nature of Magmatism in the Appalachian Orogen, Geological Society of America Memoir 191*; Sinha, A.K., Whalen, J.B., Hogan, J.P., Eds.; Geological Society of America: Boulder, CO, USA, 1997; pp. 275–286.
72. Bickford, M.E.; Van Schmus, W.R.; Karlstrom, K.E.; Mueller, P.A.; Kamenov, G.D. Mesoproterozoic-trans-Laurentian magmatism: A synthesis of continent-wide age distributions, new SIMS U-Pb ages, zircon saturation temperatures, and Hf and Nd isotopic compositions. *Precambrian Res.* **2015**, *265*, 286–312. [[CrossRef](#)]
73. Van Schmus, W.R.; Bickford, M.E.; Turek, A. Proterozoic geology of the east-central Midcontinent basement. In *Basement and basins of eastern North America*; van der Pluijm, B.A., Catacosinos, P.A., Eds.; Geological Society of America: Boulder, CO, USA, 1996; pp. 7–32.

74. Sevigny, J.H.; Hanson, G.N. Orogenic evolution of the New England Appalachians of southwestern Connecticut. *Geol. Soc. Am. Bull.* **1993**, *105*, 1591–1605. [[CrossRef](#)]
75. Gower, C.F.; Krogh, T.E. A U–Pb geochronological review of the Proterozoic history of the eastern Grenville Province. *Can. J. Earth Sci.* **2002**, *39*, 795–829. [[CrossRef](#)]
76. Moecher, D.P.; Samson, S.D. Differential zircon fertility of source terranes and natural bias in the detrital zircon record: Implications for sedimentary provenance analysis. *Earth Planet. Sci. Lett.* **2006**, *247*, 252–266. [[CrossRef](#)]
77. Osberg, P.H.; Tull, J.F.; Robinson, P.; Hon, R.; Butler, J.R. The Acadian orogen. In *The Appalachian–Ouachita Orogen in the United States*; Hatcher, R.D., Jr., Thomas, W.A., Viele, G.W., Eds.; Geological Society of America: Boulder, CO, USA, 1989; pp. 179–232.
78. Becker, T.P.; Thomas, W.A.; Samson, S.D.; Gehrels, G.E. Detrital zircon evidence of Laurentian crustal dominance in the lower Pennsylvanian deposits of the Alleghanian clastic wedge in eastern North America. *Sediment. Geol.* **2005**, *182*, 59–86. [[CrossRef](#)]
79. Coleman, J.L.; Cahan, S.M. *Preliminary Catalog of the Sedimentary Basins of the United States, USGS Open-File Report 2012-111*; U. S. Geological Survey: Reston, VA, USA, 2012.
80. Gleason, J.D.; Finney, S.C.; Gehrels, G.E. Paleotectonic implications of a Mid- to Late-Ordovician provenance shift, as recorded in sedimentary strata of the Ouachita and southern Appalachian Mountains. *J. Geol.* **2002**, *110*, 291–304. [[CrossRef](#)]
81. Milliman, J.D.; Syvitski, J.P.M. Geomorphic/tectonic control of sediment discharge to the ocean: The importance of small mountainous rivers. *J. Geol.* **1992**, *100*, 525–544. [[CrossRef](#)]
82. Chang, Z.; Vervoort, J.D.; McClelland, W.C.; Knaack, C. U-Pb dating of zircon by LA-ICP-MS. *Geochem. Geophys. Geosystems* **2006**, *7*. [[CrossRef](#)]
83. Gehrels, G.; Valencia, V.; Pullen, A. Detrital Zircon Geochronology by Laser-Ablation Multicollector ICPMS at the Arizona LaserChron Center. *Paleontol. Soc. Pap.* **2006**, *12*, 67–76. [[CrossRef](#)]
84. Gehrels, G.E.; Valencia, V.A.; Ruiz, J. Enhanced precision, accuracy, efficiency, and spatial resolution of U-Pb ages by laser ablation-multicollector-inductively coupled plasma-mass spectrometry. *Geochem. Geophys. Geosyst.* **2008**, *9*, 1–13. [[CrossRef](#)]
85. Corfu, F.; Davis, D.W. A U-Pb geochronological framework for the western Superior Province. In *Geology of Ontario*; Thurston, P.C., Williams, H.R., Sutcliffe, R.H., Stott, G.M., Eds.; Ontario Geological Survey: Toronto, ON, Canada, 1992; pp. 1335–1346.
86. Böhm, C.O.; Heaman, L.M.; Creaser, R.A.; Corkery, M.T. Discovery of pre-3.5 Ga exotic crust at the northwestern Superior Province margin, Manitoba. *Geology* **2000**, *28*, 75–78. [[CrossRef](#)]
87. David, J.; Parent, M.; Stevenson, R.; Nadeau, P.; Godin, L. The Porpoise Cove supracrustal sequence, Inukjuak area: A unique example of Paleoarchean crust (ca. 3.8 Ga) in the Superior Province. *Geol. Assoc. Canada Progr. Abstr.* **2003**, *28*, 355.
88. Percival, J.A.; Helmstaedt, H. Insights on Archean continent—Ocean assembly, western Superior Province, from new structural, geochemical and geochronological observations: Introduction and summary. *Precambrian Res.* **2004**, *132*, 209–212. [[CrossRef](#)]
89. Bickford, M.E.; Wooden, J.L.; Bauer, R.L. SHRIMP study of zircons from Early Archean rocks in the Minnesota River Valley: Implications for the tectonic history of the Superior Province. *Bull. Geol. Soc. Am.* **2006**, *118*, 94–108. [[CrossRef](#)]
90. Langford, F.F.; Morin, J.A. The development of the Superior province of northwestern Ontario by merging island arcs. *Am. J. Sci.* **1976**, *276*, 1023–1034. [[CrossRef](#)]
91. Calvert, A.J.; Ludden, J.N. Archean continental assembly in the southeastern Superior Province of Canada. *Tectonics* **1999**, *18*, 412–429. [[CrossRef](#)]
92. Sims, P.K. Early Proterozoic Penokean orogen. In *Archean and Proterozoic Geology of the Lake Superior Region, USA: 1993; USGS Professional Paper 1556*; Sims, P.K., Carter, L.M.H., Eds.; United States Government Printing Office: Washington, DC, USA, 1996; pp. 28–30.
93. Holm, D.K. A geodynamic model for Paleoproterozoic post-tectonic magma genesis in the southern Trans-Hudson (Black Hills, South Dakota) and Penokean (southern Lake Superior) orogens. *Rocky Mt. Geol.* **1999**, *34*, 183–194. [[CrossRef](#)]
94. Chandler, V.W.; Boerboom, T.J.; Jirsa, M.A. Penokean tectonics along a promontory-embayment margin in east-central Minnesota. *Precambrian Res.* **2007**, *157*, 26–49. [[CrossRef](#)]

95. Craddock, J.P.; Malone, D.H.; Schmitz, M.D.; Gifford, J.N. Strain variations across the Proterozoic Penokean Orogen, USA and Canada. *Precambrian Res.* **2018**, *318*, 25–69. [[CrossRef](#)]
96. Van Schmus, W.R.; Bickford, M.E.; Zietz, I. Early and middle Proterozoic provinces in the central United States. In *Proterozoic Lithosphere Evolution*; Kroner, A., Ed.; American Geophysical Union: Washington, DC, USA, 1987; p. 273.
97. Bennett, V.C.; DePaolo, D.J. Proterozoic crustal history of the western United States as determined by neodymium isotopic mapping. *Bull. Geol. Soc. Am.* **1987**, *99*, 674–685. [[CrossRef](#)]
98. Condie, K.C. Proterozoic terranes and continental accretion in southwestern North America. In *Proterozoic Crustal Evolution*; Condie, K.C., Ed.; Elsevier: Amsterdam, The Netherlands, 1992; pp. 447–480.
99. Rämö, O.T.; McLemore, V.T.; Hamilton, M.A.; Kosunen, P.J.; Heizler, M.; Haapala, I. Intermittent 1630–1220 Ma magmatism in central Mazatzal province: New geochronologic piercing points and some tectonic implications. *Geology* **2003**, *31*, 335–338. [[CrossRef](#)]
100. Freiburg, J.T.; McBride, J.H.; Malone, D.H.; Leetaru, H.E. Petrology, geochronology, and geophysical characterization of Mesoproterozoic rocks in central Illinois, USA. *Geosci. Front.* **2019**. [[CrossRef](#)]
101. Xie, X.; Buratowski, G.; Manager, W.L.; Zachry, D. U-Pb Detrital-zircon Geochronology of the Middle Bloyd Sandstone (morrowan) of Northern Arkansas (USA.): Implications For Early Pennsylvanian Sediment Dispersal in the Laurentian Foreland. *J. Sediment. Res.* **2018**, *88*, 795–810. [[CrossRef](#)]
102. Dennis, A.J.; Wright, J.E. The Carolina terrane in northwestern South Carolina, USA: Late Precambrian-Cambrian deformation and metamorphism in a peri-Gondwanan oceanic arc. *Tectonics* **1997**, *16*, 460–473. [[CrossRef](#)]
103. Barnett, R.S. Basement Structure of Florida and its Tectonic Implications. *GCAGS Trans.* **1975**, *25*, 122–142. [[CrossRef](#)]
104. Chowns, T.; Williams, C. Pre-Cretaceous rocks beneath the Georgia coastal plain—regional implications. In *Studies Related to the Charleston, South Carolina Earthquake of 1886—Tectonics and Seismicity*, USGS Professional Paper 1313; Gohn, G., Ed.; United States Government Printing Office: Washington, DC, USA, 1983; pp. L1–L42.
105. Duncan, J. Geologic History of an Accreted Terrane: Paleozoic Stratigraphy of the North Florida Basin, Suwannee Terrane. Ph.D. Thesis, Florida State University, Tallahassee, FL, USA, 1998.
106. Mueller, P.A.; Heatherington, A.L.; Foster, D.A.; Thomas, W.A.; Wooden, J.L. The Suwannee suture: Significance for Gondwana-Laurentia terrane transfer and formation of Pangaea. *Gondwana Res.* **2014**, *26*, 365–373. [[CrossRef](#)]
107. Cramer, F.H. Middle and upper silurian chitinozoan succession in Florida subsurface. *J. Paleontol.* **1973**, *47*, 279–288.
108. Pojeta, J. *Silurian-Devonian Pelecypods and Paleozoic Stratigraphy of Subsurface Rocks in Florida and Georgia and Related Silurian Pelecypods From Bolivia and Turkey*, USGS Professional Paper 879; United States Government Printing Office: Washington, DC, USA, 1976.
109. Opdyke, N.D.; Jones, D.S.; Macfadden, B.J.; Smith, D.L.; Mueller, P.A.; Shuster, R.D. Florida as an exotic terrane: Paleomagnetic and geochronologic investigation of lower Paleozoic rocks from the subsurface of Florida (USA). *Geology* **1987**, *15*, 900–903. [[CrossRef](#)]
110. Mueller, P.A.; Heatherington, A.L.; Wooden, J.L.; Shuster, R.D.; Nutman, A.P.; Williams, I.S. Precambrian zircons from the Florida basement: A Gondwanan connection. *Geology* **1994**, *22*, 119–122. [[CrossRef](#)]
111. Clift, P.D.; Heinrich, P.; Dunn, D.; Jacobus, A.; Blusztajn, J. The Sabine block, Gulf of Mexico: Promontory on the North American margin? *Geology* **2018**, *46*, 15–18. [[CrossRef](#)]
112. Sinha, A.K. Lead isotope mapping of crustal reservoirs within the Grenville superterrane. *Geol. Soc. Am. Abstr. Programs* **1997**, *29*, 69.
113. Chidester, A.H. Evolution of the ultramafic complexes of northwestern New England. In *Studies of Appalachian Geology: Northern and Maritime*; Zen, E., White, W.S., Hadley, J.B., Thompson, J.B., Eds.; Wiley Interscience: New York, NY, USA, 1968; pp. 343–354.
114. Naylor, R.S. A Field and Geochronologic Study of Mantled Gneiss Domes in General New England. Ph.D. Thesis, California Institute of Technology, Pasadena, CA, USA, 1967.
115. Leo, G.W.; Zartman, R.E.; Brookins, D.G. Glastonbury Gneiss and Mantling Rocks (a Modified Oliverian Dome) in South-Central Massachusetts and North-Central Connecticut: Geochemistry, Petrogenesis, and Isotopic Age. *Geol. Surv. Prof. Pap.* **1984**, *1295*, 1–45.

116. Billings, M.P. *The Geology of New Hampshire Part II-Bedrock geology*; The New Hampshire State Planning and Development Commission: Concord, NH, USA, 1956; p. 204.
117. Rankin, D.W. Volcanism related to tectonism in the Piscataquis Volcanic belt, an island arc of early Devonian age in north-central Maine. In *Studies of Appalachian Geology: Northern and Maritime*; Zen, E., White, W.S., Hadley, J.B., Thompson, J.B.J., Eds.; Interscience Publishers: New York, NY, USA, 1968; pp. 355–370.
118. Bradley, D.C. Tectonics of the Acadian Orogeny in New England and adjacent Canada (USA). *J. Geol.* **1983**, *91*, 381–400. [[CrossRef](#)]
119. Hon, R.; Fitzgerald, J.P.; Sargent, S.L.; Schwartz, W.D.; Dostal, J.; Keppie, J.D. Silurian-early Devonian mafic rocks of the Piscataquis volcanic belt in northern Maine. *Atl. Geol.* **1992**, *28*, 163–170. [[CrossRef](#)]
120. Berry, W.B.N.; Boucot, A.J. *Correlation of the North American Silurian Rocks*; Geological Society of America Special Papers; Geological Society of America: Boulder, CO, USA, 1970; Volume 102, p. 289. ISBN 0-8137-2102-4.
121. Shride, A.F. Stratigraphy and Correlation of the Newbury Volcanic Complex, Northeastern Massachusetts. In *Contributions to the Stratigraphy of New England: Geological Society of America Memoir 148*; Page, L.R., Ed.; Geological Society of America: Boulder, CO, USA, 1976; pp. 147–178.
122. Gates, O. Geologic Map and cross Sections of the Eastport quadrangle, Maine. Available online: https://digitalmaine.com/mgs_maps/292/ (accessed on 17 January 2020).
123. Hatcher, R.D. The Appalachian orogen: A brief summary. In *From Rodinia to Pangea: The Lithotectonic Record of the Appalachian Region, GSA Memoir 206*; Tollo, R., Bartholomew, M., Hibbard, J., Karabinos, P., Eds.; Geological Society of America: Boulder, CO, USA, 2010; pp. 1–20.
124. Hatcher, R.D. Tectonic map of the southern and central Appalachians: A tale of three orogens and a complete Wilson cycle. In *4-D Framework of Continental Crust, GSA Memoir 200*; Hatcher, R.D.J., Carlson, M.P., McBride, J.H., Martínez Catalán, J.R., Eds.; Geological Society of America: Boulder, CO, USA, 2007; pp. 595–632.
125. Hatcher, R.D.J.; Thomas, W.A.; Geiser, P.A.; Snoke, A.W.; Mosher, S.; Wiltschko, D.V. Alleghanian orogen. In *The Appalachian–Ouachita Orogen in the United States*; Hatcher, R.D.J., Thomas, W.A., Viele, G.W., Eds.; Geological Society of America: Boulder, CO, USA, 1989; pp. 233–318.



© 2020 by the authors. Licensee MDPI, Basel, Switzerland. This article is an open access article distributed under the terms and conditions of the Creative Commons Attribution (CC BY) license (<http://creativecommons.org/licenses/by/4.0/>).